Advances in Applied Mathematics and Mechanics
Adv. Appl. Math. Mech., Vol. **17**, No. 1, pp. 315-349

DOI: 10.4208/aamm.OA-2023-0195
February 2025

Exploring Acoustic and Sound Wave Propagation Simulations: A Novel Time Advancement Method for Homogeneous and Heterogeneous Media

Shashi Kumar[1], Bangaru Ramcharan[1], Vivek S. Yadav[2], Ankit Singh[2], Yogesh G. Bhumkar[1] and Manoj K. Rajpoot[2,*]

[1] *Scientific Computing Laboratory, School of Mechanical Sciences, Indian Institute of Technology Bhubaneswar, Bhubaneswar 752050, Odisha, India*
[2] *Mathematics and Computing Laboratory, Department of Mathematical Sciences, Rajiv Gandhi Institute of Petroleum Technology, Jais, Amethi 229304, UP, India*

Received 19 July 2023; Accepted (in revised version) 25 April 2024

Abstract. In this article, we have developed a new time-marching method to simulate sound and soliton propagation in homogeneous and heterogeneous media. The proposed time integration scheme can numerically preserve physical dispersion over a wide wavenumber range and conserve energy while solving wave propagation problems. Here, the Fourier stability analysis has been used to assess the numerical properties of the developed method. The proposed numerical method's dispersion and dissipation properties have also been compared with the classical fourth-order Runge-Kutta (RK4) method. Stability property contours for the newly proposed method display that the maximum allowable time step is at least five times higher than the RK4 method. The Fourier stability analysis also explains the dispersion error associated with the used spatio-temporal discretization schemes. It is observed that the dispersion error is significantly small for the proposed time integration schemes compared with the RK4 method. The proposed methods simulate sound propagation problems with fewer computational resources that otherwise demand high computational costs. The efficacy of the proposed time integration methods has been demonstrated by solving benchmark sound wave propagation problems. Moreover, to test the developed method's efficiency and robustness, we have performed simulations of the sound wave propagation in a layered media, corner-edge model, and damped sine-Gordon equation.

AMS subject classifications: 65Mxx, 76Qxx, 76B15

Key words: Time stepping, acoustic wave propagation, sound wave propagation, compact schemes, energy conservation, sine-Gordon equation.

*Corresponding author.
Emails: bhumkar@iitbbs.ac.in (Y. Bhumkar), mrajpoot@rgipt.ac.in (M. Rajpoot)

1 Introduction

Engineering problems involving sound wave propagation, reflection, diffraction, and superposition, are computationally intensive and challenging [36, 43]. Acoustic disturbances are pressure fluctuations superimposed on the background atmospheric pressure field. These pressure fluctuations' amplitude is usually a few orders smaller than the background pressure field. The viscous nature of the air does not alter the amplitudes of these fluctuations when the acoustic wave propagation is considered over a small distance [24]. The propagation of acoustic waves inside a one-dimensional (1D) domain displays a non-dissipative and non-dispersive nature. However, most of the traditional discretization schemes show a dispersive and dissipative nature across a wide wavenumber range. Dispersion and dissipation errors are usually high for the high wavenumber components when the computations are performed over large CFL (Courant-Friedrichs-Lewy) numbers. Thus, to keep dispersion and dissipation errors minimal, one is forced to compute on a highly refined grid with a significantly smaller time-step. Most of the schemes become unstable at higher CFL numbers. Thus, we have to use very small time-steps while performing computational aeroacoustic (CAA) simulations, which increases the computational cost significantly.

Simulations of some of the engineering problems, such as analysis of material defects using sound waves or sound wave propagation in seawater, involve heterogeneous mediums. Such problems pose further challenges as the medium properties change spatially, causing spatial variation in the speed of sound. One observes sound wave reflections and diffraction due to spatial gradients or discontinuities present in the medium properties. So far, we have listed computational challenges associated with linear acoustics problems where the frequency of sound waves in the domain is the same as the excitation or driving frequency. If the amplitude of the sound waves is sufficiently large, then the nonlinear effects also become important. If the frequency of the sound waves is sufficiently large, one must also consider the attenuation of sound waves due to the dissipative nature of the medium. Thus the used discretization scheme should have the ability to capture complex physical phenomena while solving the governing partial differential equations. To address these challenging issues, here we have proposed and used a new time integration scheme (EDP_1) along with the second-order centered (CD2) and sixth-order compact (C6) [26] spatial discretization schemes. Authors in [9] proposed the unconditionally positive definite finite difference (UPFD) method, which has been thoroughly validated [2] for the advection-diffusion-reaction systems. Authors in [34] developed unconditionally stable methods by utilizing the combination of the hopscotch spatial structure and leapfrog time integration to solve the time-dependent diffusion equation. Moreover, by considering odd-even hopscotch structure, authors in [35, 40] developed novel numerical methods to solve time-dependent diffusion equation. Compact difference schemes on uniform grid spacing have recently gained significant popularity for simulating flow and wave propagation problems on collocated and staggered grids [1, 19]. Regions with large gradients necessitate fine grid spacing, whereas regions

with small gradients can be adequately represented with coarser grid spacing. References [7, 21, 22, 32, 42] provide compact schemes designed for non-uniform grids. The newly proposed time integration scheme's numerical properties have been compared with the RK4 method. Solutions to some benchmark problems involving sound wave propagation in homogeneous and heterogeneous mediums are reported. Solutions for model problems in which the non-linear aspects are important are also computed using the newly proposed time integration scheme EDP_1.

Sound wave propagation equation with a non-zero point source is frequently used to model wave propagation in geophysics for underground imaging and seabed exploration. Seismic waves propagate from the earth's surface and transmit to the stratified heterogeneous media composed of ocean and atmosphere. Numerical solutions to the sound wave propagation in such heterogeneous media involve successive reflection and refraction from the interfaces, which lead to the numerical dispersion [8]. Propagation of sound waves in a heterogeneous medium brings additional complications as the phase speed of sound itself changes inside a computational domain at different locations. The conventional discretization methods introduce severe numerical dispersion. To capture the sound wave propagation accurately, dispersion relation preserving space-time accurate discretization schemes are required. As the exact solution of a seismic wave equation is generally unavailable, discretized procedures are the only practical solution for sound wave propagation in heterogeneous media. In the present study, we have considered sound wave propagation in two-layered media and the computationally challenging corner-edge model consists of a three-layered medium [47].

Solitons represent a special wave-like solution to nonlinear partial differential equations (PDEs), that propagate through the medium without undergoing any deformation due to dispersion. Furthermore, Soliton does not change its shape while interacting with other solitons. Solitons have been proven to play a crucial role in the theory of nonlinear PDEs. For a variety of equations, such as the Korteweg-de Vries equation, the sine-Gordon equation, and the nonlinear Schrödinger equation, soliton solutions have been discovered. The exact solution to the undamped sine-Gordon equation with zero damping is discussed in [15], and for the more realistic case with damping effects, analytical solutions do not exist. The presence of the damping coefficient in the sine-Gordon equation slows the propagation of the solitons without altering their shape. As energy conservation theoretically holds for the undamped sine-Gordon equation, the numerical solutions of the undamped sine-Gordon equation are used to show the nonlinear stability of the developed scheme. It is observed that in the undamped case, energy remains constant as time advances, while the presence of damping reduces energy due to dissipation as time advances. In the past, researchers have also paid attention to models admitting solitons in higher dimensions, and the model discussed in [20] can be mathematically described by the 2D sine-Gordon equation. Cui [12]used a fourth-order compact ADI scheme to solve the generalized sine-Gordon equation in 2D rectangular domains with three time-level algorithm. The error estimate was derived using the method of energy. Deng and Liang [14] derived two conditionally stable compact ADI schemes having fourth-order

accuracy in space and time for the general initial-boundary value problem of the nonlinear wave equation. The accuracy of the schemes given in [14] is validated by solving coupled sine-Gordon and damped wave equations. Moreover, solutions of sine-Gordon using thin-plate splines radial basis function are given by Dehghan and Shokri [13]. The numerical solutions are shown for the propagation of line and ring solitons.

The second-order linear wave equation dictates the evolution of sound disturbances in space and time. Thus it serves as a the model equation to understand sound wave propagation in different media as well as nonlinear diffusion problems in mathematical biology [6,11,25]. Generally, numerical solutions of PDEs with second-order derivative in time are obtained by transforming them into an equivalent first-order systems, in which time-integration is performed using Runge-Kutta (RK) or linear multistep methods [17]. However, the classical Rung-Kutta-Nyström (RKN) methods can be directly used for the time integration of the second-order time derivative. Two-derivative implicit-explicit Rung-Kutta-Nyström method for the sound and soliton propagation in heterogeneous media is given in [39].

Liao et al. [28] formulated a compact scheme for the simulations of acoustic wave propagation in a two-dimensional heterogeneous media with the ADI technique to reduce the computational cost. Authors in [28] noted that due to variable wave velocity, the use of the ADI method is arduous and presented a strategy to maintain fourth-order accuracy in space and time. Li et al. [27] extended the methodology discussed in [28] for the solution 3D acoustic wave equation. The compact difference methods provide substantial advantages over the classical finite difference methods while evaluating the spatial derivative terms. Although compact schemes have a smaller stencil, these schemes have a higher resolving ability and help us to compute the solution more accurately [30]. To avoid the difficulty of implementation of the compact scheme due to the spatially varying coefficient in the wave equation, Britt et al. [5] suggested shifting the variable coefficients with the time-derivative term. Thus, it is important to use high-resolution compact spatial difference schemes and suitable time integration schemes to compute accurately and efficiently.

In this paper, we have formulated a new time-marching method for the simulation of acoustic and soliton propagation in homogeneous and heterogeneous media. We would like to mention here that in contrast to the method given in [33], the present method uses a different approach to get the first-order system of equations having second-order spatial derivatives. The structure of the present article is as follows. In Section 2, the derivation for the new time-integration method to simulate sound propagation has been provided. Section 3 discusses the Fourier stability analysis of the developed method for numerically solving 1D wave equation. In Section 4, we have discussed results for the simulation of various test cases for sound wave propagation in a homogeneous media. Section 5 deals with the simulations of sound wave propagation in 2D heterogeneous media. In Section 6, results of the simulations of the undamped and damped sine-Gordon equation are given for various solitons cases. Furthermore, the energy conservation in the case of the damped and undamped sine-Gordon equation is discussed in Section 6. The manuscript

ends with important conclusions in Section 7.

2 Formulation of new time-integration method

In this section, we have formulated a new time-integration method for accurately and efficiently simulating the sound wave propagation problems.

2.1 One-dimensional linearized Euler equation

Here, we consider the propagation of a sound disturbance following 1D linearized Euler equations in a dimensional form. The governing equations in the Cartesian coordinates are given as [36]

$$\frac{\partial u}{\partial t}=-\frac{1}{\rho_0}\frac{\partial p}{\partial x},\quad \frac{\partial p}{\partial t}=-\gamma P_0\frac{\partial u}{\partial x}, \tag{2.1}$$

where p (pressure) and u (velocity) are the acoustic variables, ρ_0 is the density of air at a given temperature, P_0 is the atmospheric pressure, and γ is the ratio of specific heats for air. Eq. (2.1) can be rewritten as

$$\frac{\partial^2 p}{\partial t^2}=c^2\frac{\partial^2 p}{\partial x^2}, \tag{2.2}$$

where c is the phase speed of sound given as $c=\sqrt{\gamma P_0/\rho_0}$. Substituting, $z=\frac{\partial p}{\partial t}$, Eq. (2.2) can be rewritten as

$$\frac{\partial z}{\partial t}=c^2\frac{\partial^2 p}{\partial x^2},\quad \frac{\partial p}{\partial t}=z, \tag{2.3}$$

with z representing the pressure variations over time. Finally, the first-order energy and dispersion relation preserving time-marching method (EDP$_1$) for the system in Eq. (2.3), is given as

$$z^{n+1}=z^n+c^2\Delta t p^n_{xx}, \tag{2.4a}$$

$$p^{n+1}=p^n+\Delta t(c_1 z^n+(1-c_1)z^{n+1}). \tag{2.4b}$$

Here Δt is the time-step, n is the time-level, and c_1 is a free parameter whose optimized value is obtained by evaluating the numerical properties of the schemes [33]. The consistency analysis of the EDP$_1$ method is given in Appendix.

2.2 Two-dimensional wave equation

To understand the performance of newly proposed numerical methods while solving CAA problems, we have considered the two-dimensional wave equation as a model equation which is given as

$$\frac{\partial^2 u}{\partial t^2}=c^2(x,y)\left(\frac{\partial^2 u}{\partial x^2}+\frac{\partial^2 u}{\partial y^2}\right),\quad (x,y)\in\Omega,\quad t\in(0,T], \tag{2.5}$$

where $c(x,y)$ represents the phase speed and indicates sound propagation in an inhomogeneous medium. Substituting,

$$v=\frac{1}{c^2(x,y)}\frac{\partial u}{\partial t},$$

Eq. (2.5) can be rewritten as

$$\frac{\partial v}{\partial t}=c^2(x,y)\left(\frac{\partial^2 u}{\partial x^2}+\frac{\partial^2 u}{\partial y^2}\right), \tag{2.6a}$$

$$\frac{\partial u}{\partial t}=v. \tag{2.6b}$$

The first-order energy and dispersion relation preserving method (EDP_1) for the system (2.6) is given as

$$v^{n+1}=v^n+\Delta t c^2(x,y)\left(u^n_{xx}+u^n_{yy}\right), \tag{2.7a}$$

$$u^{n+1}=u^n+\Delta t(c_1 v^n+(1-c_1)v^{n+1}), \tag{2.7b}$$

where c_1 is a free parameter whose optimum value is dictated by numerical properties of the chosen discretization schemes [33].

3 Fourier stability analysis of 1D wave equation

To test the stability of the developed method, we have performed Fourier stability analysis [41, 46] for the system of equations given in Eq. (2.3) with periodic boundary conditions. The unknown $u(x,t)$ can be represented as, $u(x,t)=\int \hat{U}e^{ikx}dk$ by using the Fourier-Laplace transform. Here, k indicates wavenumber while $\hat{U}$ indicates the spectral amplitude of the variable $u(x,t)$. The first and second-order exact space derivatives are calculated as

$$u_x(x,t)|_{exact}=\int ik\hat{U}(k,t)e^{ikx}dk,$$

$$u_{xx}(x,t)|_{exact}=\int(-k^2)\hat{U}(k,t)e^{ikx}dk.$$

However, when the same derivatives are evaluated numerically using difference schemes, one commits numerical error as higher-order derivative terms in the Taylor series expansion are truncated. Thus numerically estimated spatial derivative differs from the exact one, and one can express the numerically evaluated first and second-order spatial derivatives as

$$u_x(x,t)|_{num}=\int ik_{eq}\hat{U}(k,t)e^{ikx}dk,$$

$$u_{xx}(x,t)|_{num}=\int(-k^2_{eq})\hat{U}(k,t)e^{ikx}dk,$$

where k_{eq} is the equivalent wavenumber and accounts for the difference between the exact and the numerically computed spatial derivative. By taking Fourier-Laplace transform of Eq. (2.4), we obtained

$$\hat{Z}^{n+1} = \hat{Z}^n - c^2 \Delta t k_{eq}^2 \hat{P}^n, \tag{3.1a}$$

$$\hat{P}^{n+1} = \hat{P}^n + \Delta t (c_1 \hat{Z}^n + (1-c_1)\hat{Z}^{n+1}), \tag{3.1b}$$

where, $\hat{P}$ and $\hat{Z}$ represent the Fourier transforms of p and z respectively. One can derive a relation between $(n+1)^{th}$ and $(n)^{th}$ time-levels from Eq. (3.1), as [33,38]

$$\hat{Y}^{n+1} = M\hat{Y}^n,$$

where,

$$\hat{Y} = (\hat{Z}, \hat{P})^T \quad \text{and} \quad M = \begin{bmatrix} 1 & -c^2\Delta t k_{eq}^2 \\ \Delta t & 1 - c^2 \Delta t^2 (1-c_1) k_{eq}^2 \end{bmatrix}.$$

The eigenvalues of the evolution matrix (M) are the amplification factor $G = [G_{N1}, G_{N2}]^T$ for EDP$_1$ method. Furthermore, by substituting $k_{eq}^2 = \frac{k_{eq}^{[2]}}{\Delta x^2}$ the eigenvalues of the evolution matrix M are obtained as

$$G_{N1,2} = e_1 \pm \frac{N_c}{2}\sqrt{e_2} \tag{3.2}$$

with

$$e_1 = \frac{-N_c^2 k_{eq}^{[2]}}{2} + \frac{N_c^2 k_{eq}^{[2]} c_1}{2} + 1,$$
$$e_2 = k_{eq}^{[2]} \left(k_{eq}^{[2]} N_c^2 c_1^2 - 2k_{eq}^{[2]} N_c^2 c_1 + k_{eq}^{[2]} N_c^2 - 4 \right),$$

where $k_{eq}^{[2]} = \phi(k\Delta x)$ with $\phi(k\Delta x)$ representing the nondimensional equivalent wavenumber, Δx is mesh-width and N_c is the CFL number defined as, $N_c = c\Delta t/\Delta x$. Using Eq. (3.2), the condition for the wave-like solutions for the model system given in Eq. (2.3) is given as, $e_2 < 0$. Moreover, the stability condition for the discretized system (2.4) using Eq. (3.2) is given as, $|G| \leq 1$.

Spatial discretization of the second-order derivative is performed using second-order centered (CD2) and the sixth-order compact (C6) [26] schemes. Stencils for (CD2) and (C6) schemes are given as

$$u_i''\big|_{CD2} = \frac{u_{i-1} - 2u_i + u_{i+2}}{\Delta x^2},$$
$$\left(\frac{2}{11} u_{i-1}'' + u_i'' + \frac{2}{11} u''_{i+1} \right)\Bigg|_{C6} = \frac{3}{11}\left(\frac{u_{i-2} - 2u_i + u_{i+2}}{4\Delta x^2} \right) + \frac{12}{11}\left(\frac{u_{i-1} - 2u_i + u_{i+2}}{\Delta x^2} \right).$$

Nondimensional equivalent wavenumbers for the (CD2) and (C6) schemes are given as

$$\phi(k\Delta x)_{\mathrm{CD2}}=2(1-\cos(k\Delta x)),\quad \phi(k\Delta x)_{\mathrm{C6}}=\frac{3\cos(2k\Delta x)+48\cos(k\Delta x)-51}{8\cos(k\Delta x)+22}.$$

We have also compared the numerical properties of the EDP$_1$ method with the RK4 method. The numerical amplification factors for the RK4 method are given as

$$G_{N1,2}\big|_{RK4}=1-\frac{N_c^2(k_{eq}^{[2]})^2}{2}+\frac{N_c^4(k_{eq}^{[2]})^4}{24}\pm i\left(N_c k_{eq}^{[2]}-\frac{N_c^3(k_{eq}^{[2]})^3}{6}\right).$$

Numerical phase shift is given as, $\beta=\arctan\left(\frac{G_{Ni}}{G_{Nr}}\right)$, where, G_{Nr} and G_{Ni} represent the real and imaginary parts of the numerical amplification factor, respectively. The normalized numerical phase speed and group velocity are defined as,

$$\frac{c_N}{c}=\frac{\beta}{k\Delta x N_c},\quad \frac{V_{g_N}}{c}=\frac{1}{N_c}\frac{d\beta}{dk\Delta x}.$$

Contour plots showing absolute values of amplification factor ($|G_N|$), normalized phase speed (c_N/c) and group velocity (V_{g_N}/c) for EDP$_1$-CD2 and EDP$_1$-C6 schemes are shown in Fig. 1 using indicated schemes. Left-column frames correspond to the EDP_1-CD2 scheme, middle-column frames correspond to the EDP$_1$-C6 scheme and right-column frames show the numerical properties using the RK4-C6 scheme. The shaded area in Fig. 1 corresponds to non-hyperbolic regions and the dotted area in the top frames represents the neutrally stable ($|G|=1$) regions for the indicated schemes. Comparison of the numerical properties shown in middle-column and right-column frames of Fig. 1 confirms that for the EDP$_1$-C6 have neutrally stable region up to $N_c=0.7614$ while for the RK4-C6 it is up to $N_c=0.1$. The developed EDP$_1$ method achieved neutral stability over a larger value of N_c as compared to the RK4 method, which allows the EDP$_1$ scheme to compute with a larger time-step. Property contours also confirm that the present EDP$_1$ methods have better stability and dispersion properties with less computational complexity as compared to the RK4 method. From the phase speed and group velocity contours shown in Fig. 1, it is evident that the C6 scheme introduces less dispersion and phase mismatch errors as compared to the CD2 scheme with a minor reduction in the neutrally stable region.

3.1 Optimization problem to determine the values for free parameter

An optimization problem, as discussed in [33], is considered to fix the value of the free parameter present in the EDP$_1$ method to improve stability and dispersion properties. Here, we have considered the following objective functions given as

$$\Psi(c_1,N_c)=\int_0^{\alpha}|G_N-G_{\mathrm{exact}}|^2 d(kh) \tag{3.3}$$

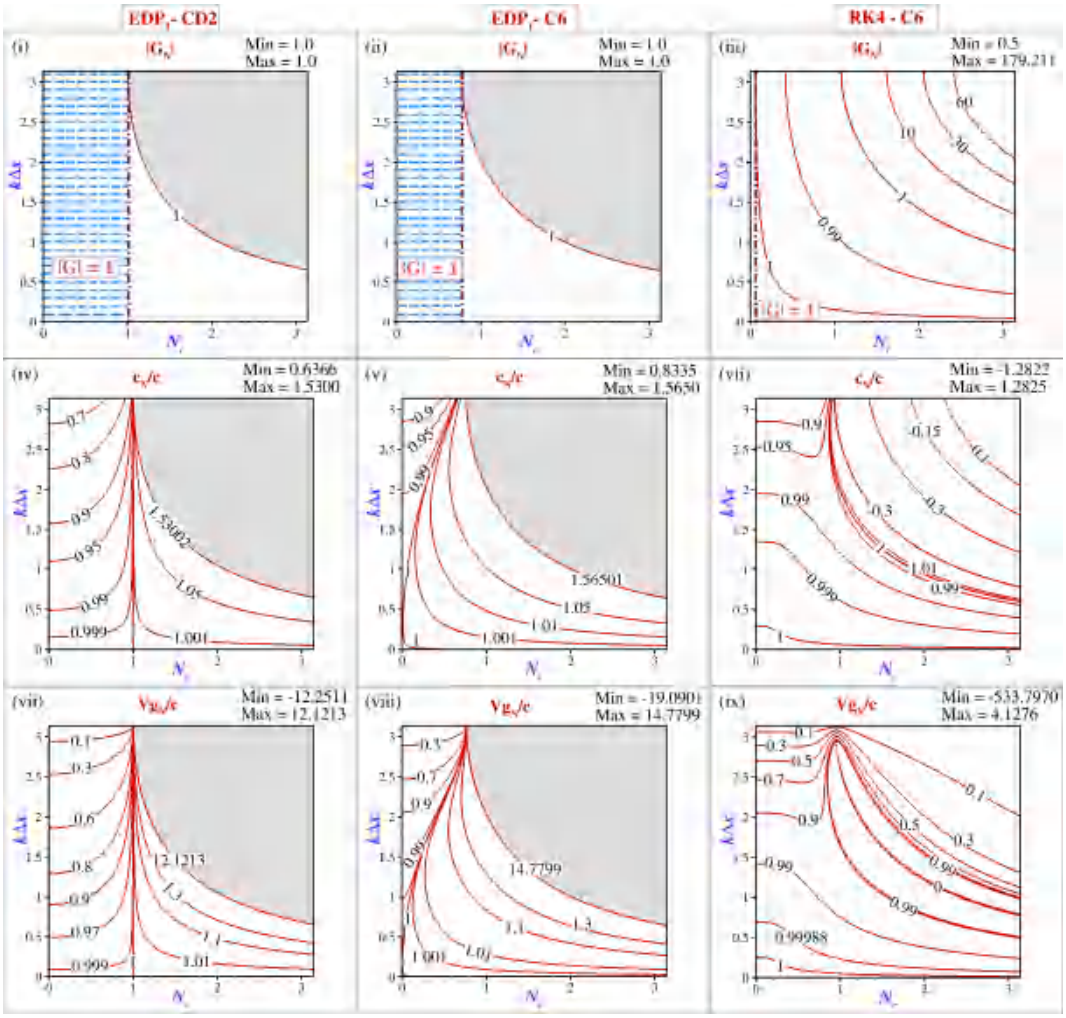

Figure 1: Contour plots showing $|G_N|$, c_N/c and Vg_N/c for Eq. (2.3) using indicated schemes. Here, the dotted area represents the neutrally stable ($|G_N|=1$) region with vertical dash-dotted line (in the top frames) mark the corresponding $(N_c)_{\text{cr}}$ and the shaded area represents the corresponding non-hyperbolic region. Contour plots for the EDP$_1$ method correspond to free parameter value $c_1 = 1.48\times10^{-4}$, as given in Table 1.

where G_N is the numerical amplification factor and

$$G_{\text{exact}} = e^{iN_c k\Delta x}$$

is the exact amplification factor. The objective function given in Eq. (3.3) is also subjected to the following constraints [33], given as

$$\psi_1(c_1, N_c) = \int_0^{\alpha_1} \big||G_N|-1\big| d(kh) \le \epsilon_1, \tag{3.4a}$$

$$\psi_2(c_1,N_c)=\int_0^{\alpha_2}\left|\left(\frac{Vg_N}{c}\right)-1\right|d(kh)\leq\epsilon_2, \tag{3.4b}$$

$$\psi_3(c_1,N_c)=\int_0^{\alpha_3}\left|\left(\frac{c_N}{c}\right)-1\right|d(kh)\leq\epsilon_3, \tag{3.4c}$$

here, α_i and ϵ_i are the admissible error tolerances. The specific values of ϵ_i have been selected according to the discussion in [33]. This process involves systematically exploring the parameter space while keeping the value of N_c constant at an arbitrary but fixed value. The inclusion of constraints specified in Eq. (3.4) transforms the optimization problem described by Eqs. (3.3)-(3.4) into a Pareto front optimization problem. The optimal values of the free parameter c_1 are given in Table 1 corresponding to $1D$ system of the equation given by Eq. (2.3).

Table 1: Optimal values of free parameter c_1 for the discretized system in Eq. (2.4) using EDP$_1$-CD2 and EDP$_1$-C6 schemes. Here, $(N_c)_{\text{cr}}$ denotes the threshold value of N_c up to which method (2.4) is neutrally stable.

c_1	EDP$_1-$CD2			EDP$_1-$C6		
	Min ($\lvert G\rvert$)	Max ($\lvert G\rvert$)	$(N_c)_{\text{cr}}$	Min ($\lvert G\rvert$)	Max ($\lvert G\rvert$)	$(N_c)_{\text{cr}}$
-0.001000	0.998000	1.000000	0.486200	0.998000	1.000000	0.380700
0.000148	**1.000000**	**1.000000**	**1.000700**	**1.000000**	**1.000000**	**0.761400**
0.001000	1.000000	1.002000	0.500200	1.000000	1.002000	0.376300
0.010000	1.000000	1.020200	0.150300	1.000000	1.020200	0.122400
0.015000	1.000000	1.030500	0.127000	1.000000	1.030700	0.099000
0.100000	1.000000	1.222200	0.049100	1.000000	1.222200	0.037400

4 Sound propagation in a homogeneous media

Numerical properties of the EDP$_1$-$C6$ method were shown in the middle-column frames of Fig. 1 which displayed the ability of the newly proposed time integration scheme to compute at a higher CFL number without experiencing numerical instability. This is an interesting feature of the proposed EDP$_1$-$C6$ scheme over the traditionally used RK4-C6 scheme as it helps to reduce the computational cost significantly. To test the efficiency and robustness of the proposed method, we have solved several benchmark problems involving sound wave propagation in a homogeneous medium. Solutions to these benchmark cases are discussed next.

4.1 Sound wave propagation in 1D domain

Here we have considered a sound wave propagation inside a 1D domain $-7.5\leq x$ and $x\geq 7.5$. The domain has been divided into 1001 equispaced grid points. The mean density and the background atmospheric pressure have been prescribed as $\rho_0=1.225\text{kg/m}^3$

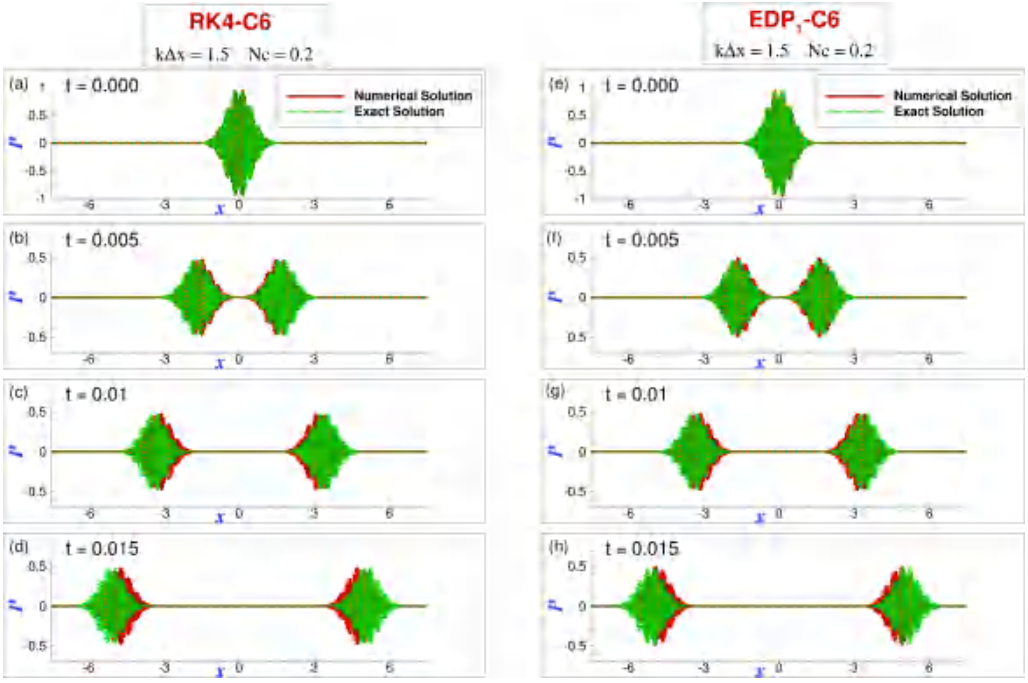

Figure 2: Solutions of 1D wave equation (2.3) have been shown for the indicated discretization schemes. Simulations have been performed for the CFL number $N_c = 0.2$ and non-dimensional wavenumber $k\Delta x = 1.5$. Dashed lines show the exact solution. Solutions with the EDP$_1$ method are computed with free parameter value $c_1 = 1.48 \times 10^{-4}$, as given in Table 1.

and $P_0 = 101325$Pa, respectively. The ratio of the specific heats is $\gamma = 1.4$ and the mean temperature is $T = 288$K. The sound wave in the form of disturbance in pressure has been centered in the domain $(x = 0)$ initially, and the corresponding initial condition is given as

$$p^0 = e^{-2x^2} \cos(k\Delta x \times x/\Delta x), \quad u^0 = 0, \tag{4.1}$$

where p^0 and u^0 provide initial conditions for the disturbance pressure and velocity fields, respectively. At the boundaries of the domain, reflecting boundary conditions are applied using Neumann boundary conditions. The parameter kh refers to the non-dimensional wavenumber, where Δx is the uniform grid spacing. To check the performance of the newly proposed time integration scheme, we have simulated sound wave propagation in a 1D domain using EDP$_1$-C6 and RK4-C6 schemes. An initial condition corresponding to the wave packet with wavenumber $k\Delta x = 1.5$ has been considered, and solutions are obtained for various CFL numbers $Nc = 0.01 - 0.7$. The analytical solution of this problem [36] suggests that the initial condition will split itself into two equal parts, which will travel in either direction with a constant phase speed (c) and also retain shape without undergoing any attenuation and amplification.

Fig. 2 displays solutions of 1D wave equation (2.2) using EDP$_1$-C6 and RK4-C6 schemes.

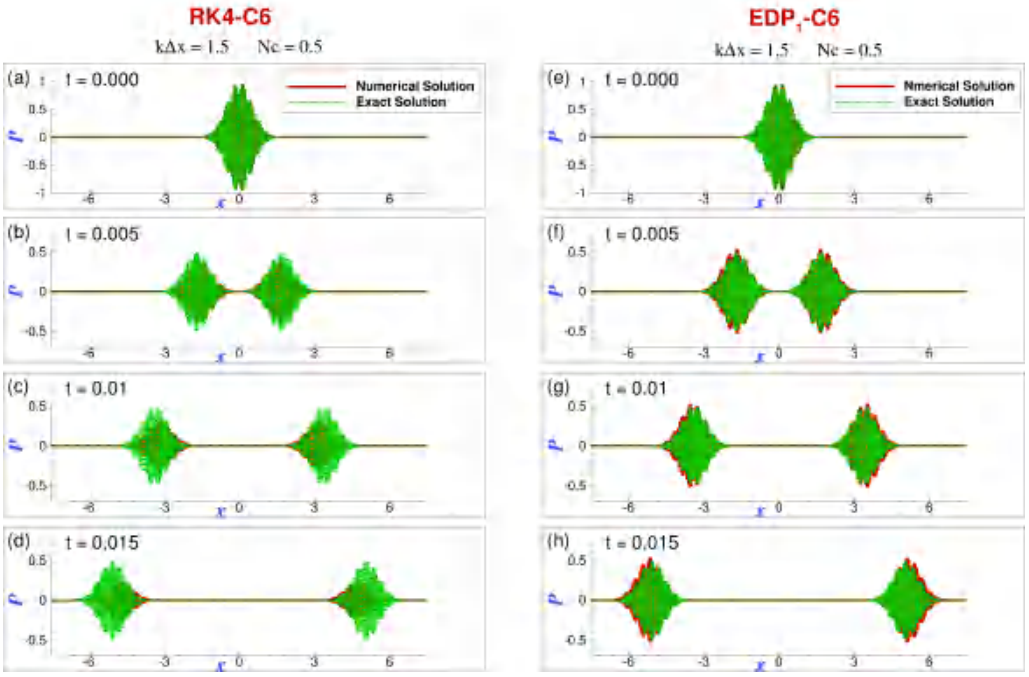

Figure 3: Solutions of 1D wave equation (2.3) with time is shown for $N_c = 0.5$ and $k\Delta x = 1.5$. Note that the solution using EDP$_1$-C6 discretization scheme display good agreement with the analytical solution while RK4-C6 scheme display significant error. Solutions with the EDP$_1$ method are computed with free parameter value $c_1 = 1.48 \times 10^{-4}$, as given in Table 1.

Dashed lines show the exact solution. Eq. (2.1) has been solved using RK4-C6 discretization scheme, while Eq. (2.2) has been solved using EDP$_1$-C6 scheme following the algorithm given in Eq. (2.4). As expected, the initial condition is split into two equal parts, each traveling in either direction. One observes that both EDP$_1$-C6 and RK4-C6 scheme computes accurately for the given conditions as the solutions match the analytical results accurately. On increasing the CFL number to $Nc = 0.5$, the solution obtained by EDP$_1$-C6 matches the analytical solution as observed from right-hand frames in Fig. 3. When the wave equation is solved with RK4-C6 with $Nc = 0.5$, we observe dissipation error as the magnitude of the obtained solution decreases compared to the exact solution as seen from left-hand frames in Fig. 3. Also, with time, dissipation error increases significantly as shown in Fig. 3(d).

By solving the $1D$ wave equations using the introduced EDP$_1$ scheme and RK4 scheme, we can conclude that for a given wave number, the EDP$_1$ scheme can solve the equations at a higher CFL number compared to RK4 time integration scheme accurately. Also, the time taken by the EDP$_1$-C6 scheme is almost 4 times less than the traditionally used RK4-C6 scheme as shown in Table 2.

Table 2: Time required in seconds to simulate a particular number of time-steps for various sound propagation problems using indicated schemes.

Problem	CFL No.	RK4-C6 (in seconds)	EDP_1-C6 (in seconds)
1D wave propagation	0.2	$\sim$2.1	$\sim$0.5
Scattering of sound from cylinder	0.4	$\sim$58.5	$\sim$13.3
Sound radiation by oscillating piston	0.13	$\sim$99.1	$\sim$23.1

4.2 Diffraction of a sound wave around a circular cylinder

Sound waves reflect and diffract around the solid object present in their path. Many engineering problems involve sound diffraction around a solid surface. The resultant sound field is dependent on the superposition of the incoming sound waves and the diffracted sound waves. The diffraction of propeller sound from an aircraft fuselage is one such example. Such a problem can be modeled by considering the diffraction of a sound wave around a circular cylinder, as discussed here. For the present problem, one needs to solve the 2D linearized Euler equations in a non-dimensional form given as [44]

$$\frac{\partial u}{\partial t}+\frac{\partial p}{\partial x}=0, \tag{4.2a}$$

$$\frac{\partial v}{\partial t}+\frac{\partial p}{\partial y}=0, \tag{4.2b}$$

$$\frac{\partial p}{\partial t}+\frac{\partial u}{\partial x}+\frac{\partial v}{\partial x}=0. \tag{4.2c}$$

Eq. (4.2) can be rewritten as

$$\frac{\partial^2 p}{\partial t^2}=\frac{\partial^2 p}{\partial x^2}+\frac{\partial^2 p}{\partial y^2}. \tag{4.3}$$

Substituting, $z=\frac{\partial p}{\partial t}$, Eq. (4.3) can be rewritten as

$$\frac{\partial z}{\partial t}=\frac{\partial^2 p}{\partial x^2}+\frac{\partial^2 p}{\partial x^2}, \tag{4.4a}$$

$$\frac{\partial p}{\partial t}=z. \tag{4.4b}$$

Algorithm for solving new first-order coupled PDEs in Eqs. (4.4) is given as

$$z^{n+1}=z^n+\Delta t(p^n_{xx}+p^n_{yy}), \tag{4.5a}$$

$$p^{n+1}=p^n+\Delta t(c_1 z^n+(1-c_1)z^{n+1}). \tag{4.5b}$$

The computational domain for this problem consists of a cylinder with a unit diameter positioned at the origin as shown in Fig. 4. An acoustic source is located at the point

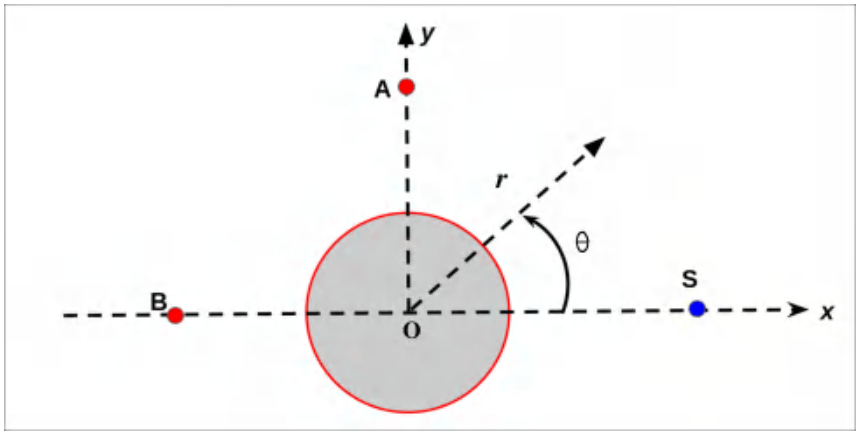

Figure 4: Schematic for sound scattering from a solid cylinder.

$S(4,0)$. Here, r and θ represent any arbitrary point's radial and angular positions in the domain, respectively. The acoustic disturbance originating at the sound source propagates toward the cylinder as time progresses. The surface of the cylinder is considered to be purely reflecting. Two points A and B with coordinates as $A(r=5,\ \theta=90^\circ)$ and $B(r=5,\ \theta=180^\circ)$ are considered to measure the time history of pressure pulse and compare with the analytical results [44]. The initial condition of the sound wave originating from the sound source is given as,

$$p^o=\exp\left[-\ln 2\left(\frac{(x-4)^2+y^2}{(0.2^2)}\right)\right].$$

To solve this problem numerically, an O-grid domain with a domain diameter equal to 15 times the diameter of the cylinder has been considered. There are 201 equispaced grid points along the radial direction and 201 equispaced grid points in the azimuthal direction. The used time-step $\Delta t=0.005$ is such that the CFL number is close to ~ 0.4. The minimum distance along the cylindrical surface is 0.016 and the minimum distance along the radial direction is 0.04. At the far field of the domain, radiative boundary conditions have been implemented while reflecting, and non-penetrating boundary conditions are implemented at the cylinder surface [44].

Computations have been carried out using the EDP_1 scheme for time advancement, and spatial derivatives are evaluated using the C6 scheme. The problem has also been solved numerically using the RK4 time-integration scheme to compare computational performance with that of the new time-integration method (EDP_1). Fig. 5 displays the sound pressure contours obtained through present simulations. Fig. 5(a) displays the instantaneous contours of sound pressure as given in Tam et al. [44] at non-dimensional time $t=7$ while Figs. 5(b) and (c) display the present simulated results using EDP_1-C6 and RK4-C6 schemes, respectively at a non-dimensional time $t=7$. One can observe that

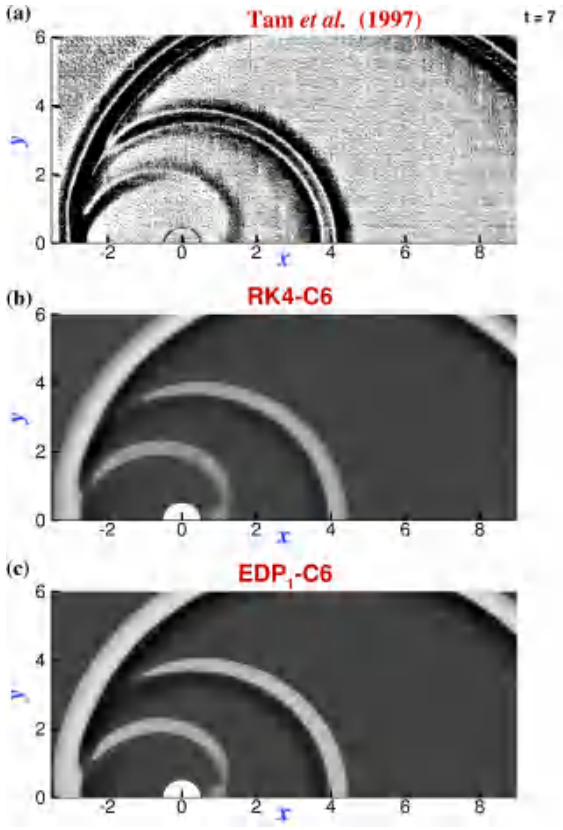

Figure 5: Qualitative comparison of diffraction of the acoustic pressure pulse from a reflecting cylinder surface. Frame (a) depicts the results taken from the literature [44]. Frames (b) and (c) display the computational results obtained using EDP_1-C6 and RK4-C6 schemes, respectively.

both the schemes predict similar waveforms given by Tam et al. [44] at the given instant. The time history of the variations of the sound pressure amplitude at locations A and B are shown in Figs. 6(a) and (b), respectively. The frame (a) displays two peaks in the time history of pressure variation. The first pressure peak is observed when the pressure pulse reaches location A directly from the sound source. Due to the diffraction of the pressure pulse around the cylinder, the second peak appears. The frame (b) displays only a single peak in the pressure history for location B, which is due to the diffraction of the sound wave around a cylinder. Thus, we conclude that the phase and amplitudes of the sound pressure waves have been predicted accurately by using the EDP_1 and RK4 schemes are in good agreement with the analytical results [44]. As the refined grid has been used for simulation, the resultant non-dimensional wavenumber is small and both the schemes display good results. However, the computational time of the EDP_1 scheme is 4 times smaller than the RK4 scheme as displayed in Table 2.

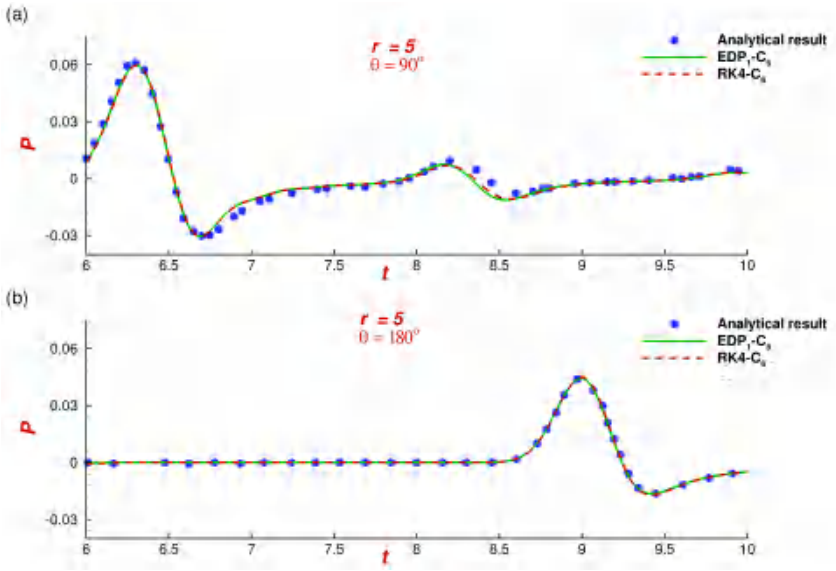

Figure 6: Quantitative comparison of time histories of sound pressure variation at indicated locations obtained using EDP_1-C6 and RK4-C6 schemes

4.3 Sound radiation by an oscillating circular piston

Here we consider the generation and propagation of sound waves due to an oscillating piston. The oscillating piston creates disturbances in pressure in the form of alternate compression and rarefaction regions. These disturbances in pressure travel throughout the domain in the form of sound waves. The schematic of the computational domain has been shown in Fig. 7. An oscillating piston is placed at the origin within a domain identified as $-150\leq r\leq 150$ and $0\leq y\leq 300$. The diameter of the piston is considered as 20, and it oscillates about the mean position located at $y=0$ as shown in Fig. 7. Here, non-dimensional linearized axisymmetric Euler equations have been solved in the cylindrical coordinates. These equations are given as [16],

$$\begin{aligned}&\frac{\partial u}{\partial t}+\frac{\partial p}{\partial r}=0,\\&\frac{\partial v}{\partial t}+\frac{\partial p}{\partial y}=0,\\&\frac{\partial p}{\partial t}+\frac{\partial u}{\partial r}+\frac{\partial v}{\partial y}+\frac{u}{r}=0.\end{aligned}$$

These equations can be written as,

$$\frac{\partial^2 p}{\partial t^2}=\frac{\partial^2 p}{\partial r^2}+\frac{\partial^2 p}{\partial y^2}+\frac{1}{r}\frac{\partial p}{\partial r}. \tag{4.6}$$

The boundary conditions along $y=0$ are given as,

$$v=0, \quad |r|>10,$$
$$v=0.0001\sin\left(\frac{\pi t}{5}\right), \quad -10\leq r\leq 10.$$

Substituting, $z=\frac{\partial p}{\partial t}$, Eq. (4.6) can be rewritten as

$$\frac{\partial z}{\partial t}=\frac{\partial^2 p}{\partial x^2}+\frac{\partial^2 p}{\partial r^2}+\frac{p_r}{r}, \tag{4.7a}$$
$$\frac{\partial p}{\partial t}=z. \tag{4.7b}$$

Algorithm of new first-order for Eqs. (4.7) method is written as

$$z^{n+1}=z^n+\Delta t\left(p^n_{xx}+p^n_{rr}+\frac{p^n_r}{r}\right), \tag{4.8a}$$
$$p^{n+1}=p^n+\Delta t(c_1 z^n+(1-c_1)z^{n+1}). \tag{4.8b}$$

The computational domain has been divided into a very fine grid into 400×401 number of grid points. The system of Eq. (4.8) has been solved using the proposed EDP_1 time advancement scheme with the parameter $c_1=0$. Computations have been performed at two different time-steps ($\Delta t=0.1$ and 0.5). Simulation results obtained using the EDP_1 time integration scheme have been compared with the results obtained using the RK4 scheme. The spatial discretization has been obtained using the *C*6 scheme. The pressure contours are shown at a non-dimensional time $t=100$ in Fig. 8 (a) and (b) for EDP_1-C6 and RK4-C6 schemes, respectively for $\Delta t=0.1$ and $Nc=0.13$. The instantaneous pressure amplitude variation along the line $r=0$ at time $t=100$ has also been compared with the analytical solution given in Fung et al. [16] as shown in Fig. 8(c). It is observed that the solutions obtained using the EDP_1-C6 and RK4-C6 schemes are in good agreement with the analytical solution of Fung et al. [16]. Figure 9 represents the variations of pressure for the CFL number $Nc=0.67$ and $\Delta t=0.5$. We can observe dispersion error for the solution obtained using RK4-C6 scheme shown in Fig. 9(c) while EDP_1-C6 is still able to provide good results on comparing with the exact solution.

Next, we have compared the computational cost for the simulations computed using RK4-C6 and EDP_1-C6 schemes for the problems discussed so far. Table 2 shows the time required in seconds to simulate a particular number of time-steps for various sound propagation problems using indicated schemes. One observes that the computations performed using the EDP_1-C6 scheme are almost 4 times faster compared to the RK4-C6 scheme. This highlights the computationally efficient nature of the newly derived EDP_1 time integration scheme.

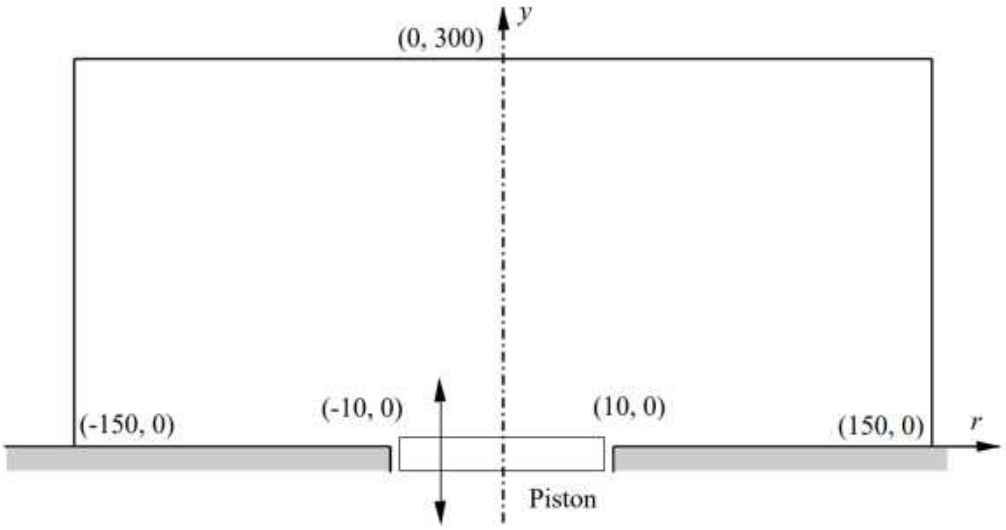

Figure 7: Schematic of domain containing an oscillating piston.

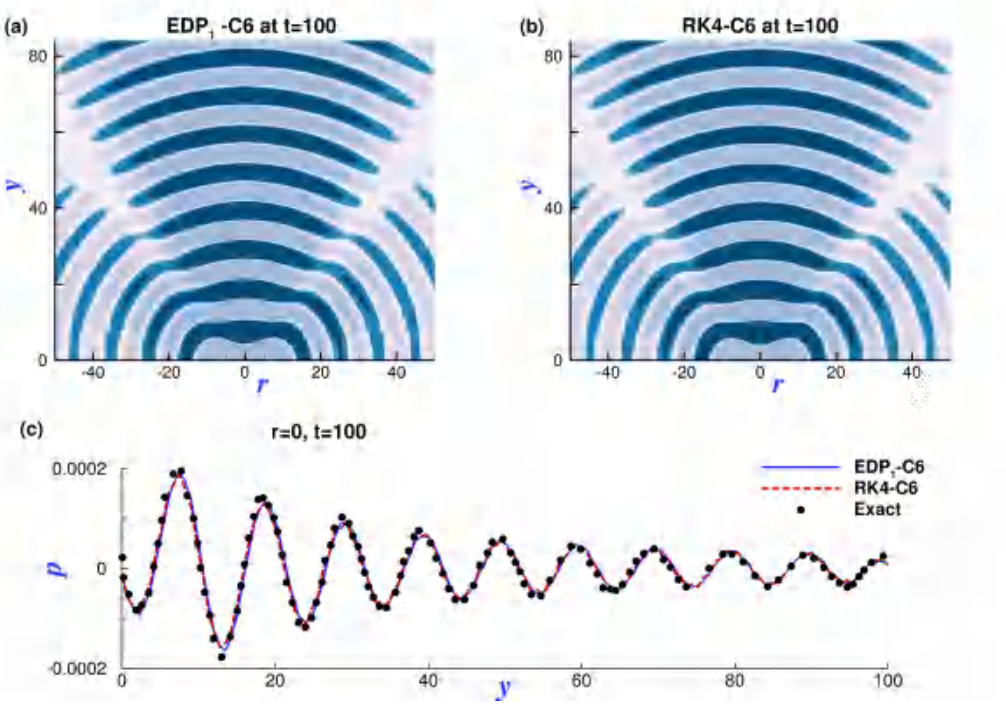

Figure 8: Acoustic pressure fields are displayed in Frames (a) and (b) for the mentioned schemes at $t=100$ and $\Delta t=0.1$. Pressure variation with time is displayed in frame (c) and compared with the exact solutions provided by Fung et al. [16].

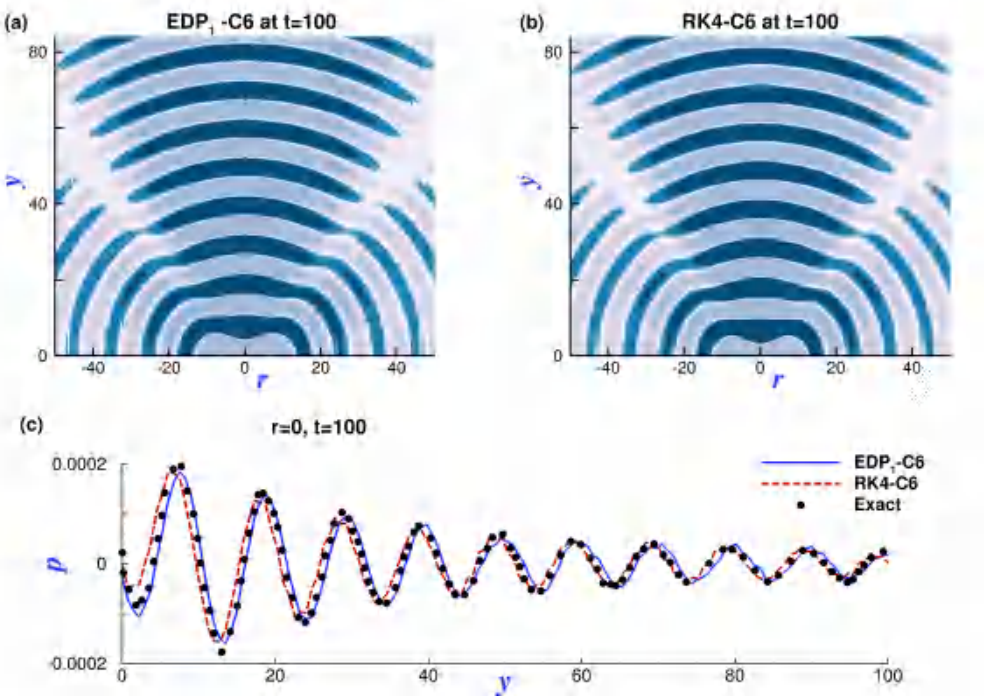

Figure 9: Frames (a) and (b) are showing the comparison of acoustic pressure fields at time $t=100$ obtained using EDP$_1$-C6 and RK4-C6 schemes respectively for $\Delta t=0.5$. (c) Pressure variation along the line $r=0$ at time $t=100$ obtained using indicated numerical schemes are compared with the exact solutions of Fung et al. [16].

4.4 Noise attenuation by thin reflecting barriers

This particular benchmark problem has been derived from earlier experimental works of Kawai [23]. This benchmark problem is designed to study the variations in diffraction and propagation of acoustic waves in the presence of a thin reflecting barrier placed in the domain. A reflecting barrier of rectangular shape with finite-thickness is placed in the computational domain as shown in Fig. 10. The range of the computational domain has been considered as $-7.5\text{m}\leq x\leq 7.5\text{m}$ along the x-direction and $-3.4\text{m}\leq y\leq 4.1\text{m}$ along the y-direction. The height of the reflecting barrier has been considered as 3.4m, and the thickness has been considered as 0.17m. The origin has been located at the top left corner of the reflecting barrier as shown in Fig. 10.

The governing equations for the propagation of acoustic waves in a dimensional form are given in [37] as

$$\frac{\partial u}{\partial t}+\frac{1}{\rho_0}\frac{\partial p}{\partial x}=0, \tag{4.9a}$$

$$\frac{\partial v}{\partial t}+\frac{1}{\rho_0}\frac{\partial p}{\partial y}=0, \tag{4.9b}$$

$$\frac{\partial p}{\partial t}+\gamma P_0\left(\frac{\partial u}{\partial x}+\frac{\partial v}{\partial y}\right)=0. \tag{4.9c}$$

Eq. (4.9) can be rewritten as

$$\frac{\partial^2 p}{\partial t^2}=\frac{\gamma P_0}{\rho_0}\left(\frac{\partial^2 p}{\partial x^2}+\frac{\partial^2 p}{\partial y^2}\right). \tag{4.10}$$

Substituting, $z=\frac{\partial p}{\partial t}$, Eq. (4.10) can be rewritten as

$$\frac{\partial z}{\partial t}=\frac{\gamma P_0}{\rho_0}\left(\frac{\partial^2 p}{\partial x^2}+\frac{\partial^2 p}{\partial y^2}\right), \quad \frac{\partial p}{\partial t}=z. \tag{4.11}$$

Algorithm of new first-order for Eqs. (4.11) method is written as

$$z^{n+1}=z^n+\frac{\Delta t\gamma P_0}{\rho_0}(p^n_{xx}+p^n_{yy}), \tag{4.12a}$$

$$p^{n+1}=p^n+\Delta t(c_1 z^n+(1-c_1)z^{n+1}). \tag{4.12b}$$

The values of parameters in the governing Eq. (4.9) are considered as $\rho_0=1.225\text{kg/m}^3$, $p_0=101325\text{N/m}^2$ and $\gamma=1.4$. The Eq. (4.10) is solved using the EDP$_1$-C6 method following the algorithm given by Eq. (4.12). The value of the free parameter is chosen as, $c_1=1.48\times10^{-4}$. The time-step used for these simulations is $\Delta t=10^{-6}$s. A monochromatic sound source with a frequency of 500Hz whose disturbance velocity, as given by

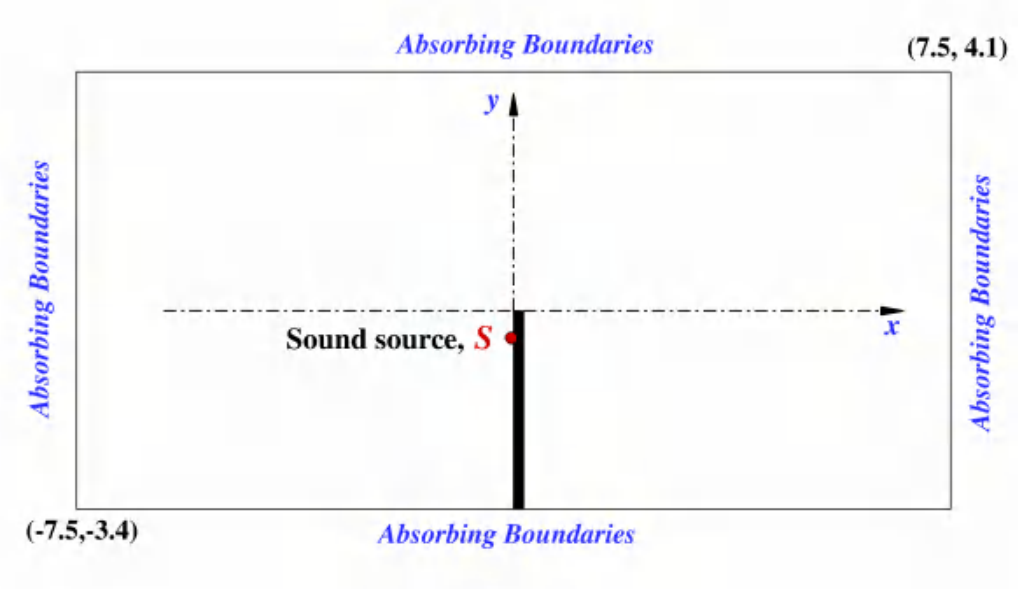

Figure 10: Schematic of the domain containing a thin reflecting barrier.

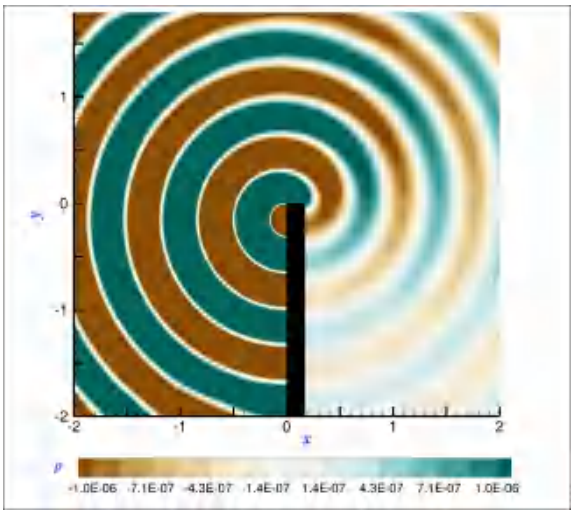

Figure 11: Acoustic pressure field obtained by the EDP$_1$-C6 scheme at a dimensional time of $t=0.009$s.

Eq. (4.13), is placed near the left top corner of the barrier at a distance of $0.17m$ from the top edge of the reflecting barrier to meet the conditions followed in the experiments of Kawai [23].

$$u(y,t)=10^{-6}\sin(2\pi 500t)\exp\left[-32(y+0.17)^2\right]. \tag{4.13}$$

The acoustic pressure field obtained numerically at time $t=0.09$s is shown in Fig. 11. Since the sound source is placed on the left side of the reflecting barrier, there is an acoustic shadow region on the right side of the barrier, as shown in Fig. 11. From the obtained acoustic pressure field, the values of sound pressure levels (SPL) in decibels (dB) are computed between the time period of 0.03s to 0.04s by considering 100 samples at different heights $(y=-1.0,-0.6,0.8,\text{and}\,1.2)$. The obtained results are compared with the experimental results [23] in Fig. 12. The present numerical results obtained using the EDP$_1$-C6 scheme are in good agreement with the experimental results [23].

5 Sound propagation in 2D heterogeneous media

Sound propagation in heterogeneous media is further computationally challenging as the sound propagation speed varies throughout the domain. In addition, depending on the individual medium characteristics such as density and sound propagation speed in a medium, part of the incident sound energy can reflect from the boundary separating two mediums. A fraction of incident sound energy can transmit across the boundary separating two mediums. Any inaccuracy associated with a numerical method will be visible from the computed solutions of such challenging problems. Thus, simulations of 2D sound wave propagation in two- and three-layered heterogeneous media have been discussed next.

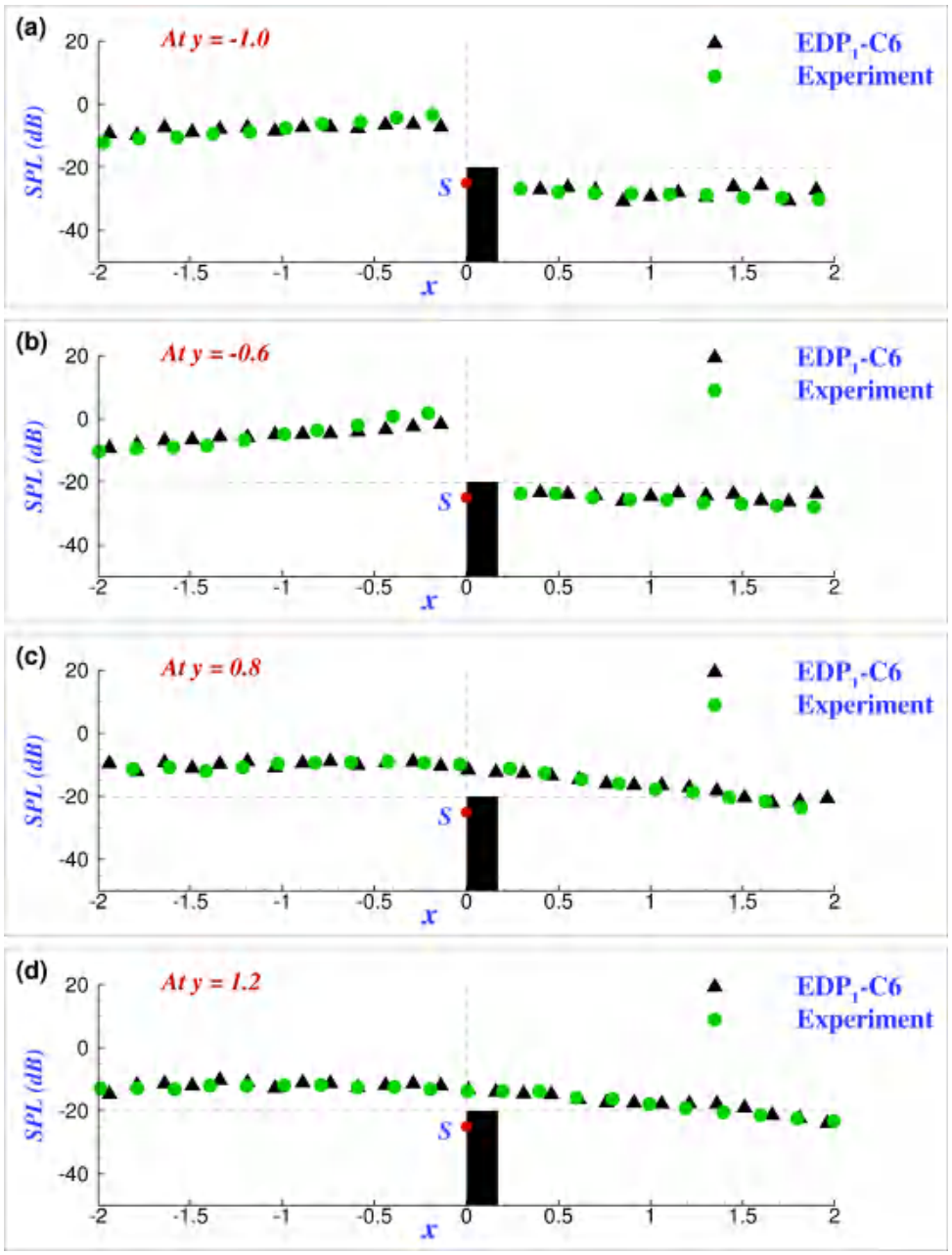

Figure 12: Sound pressure levels (in dB) obtained at different heights. Frames (a) and (b) depict the SPL values obtained below the line $y=0$, while frames (c) and (d) represent the SPL values obtained above the line $y=0$. Experimental data is reproduced from Kawai [23].

5.1 Sound propagation in two-layered media

For wave propagation in a layered medium, we have considered solving the 2D inhomogeneous wave equation given in Eq. (2.5) in the domain $[0,5000\text{m}]\times[0,5000\text{m}]$ with

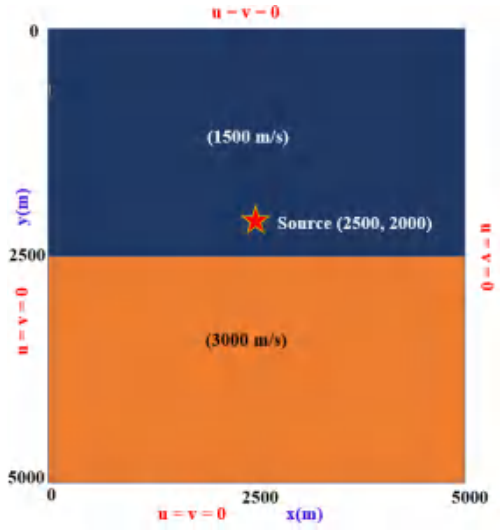

Figure 13: Schematic diagram for two-layered sound wave propagation model consisting of two homogeneous layers. Corresponding phase velocity has been indicated in respective layers. The star indicates position of the sound source.

the zero Dirichlet boundary conditions. The source function is chosen as the Ricker's wavelet [28], given as

$$f(x,y,t)=\delta(x-x_0,y-y_0)\left[1-2\pi^2 f_p^2(t-d_r)^2\right]e^{-\pi^2 f_p^2(t-d_r)^2},$$

where, $\delta(x-x_0,y-y_0)$ is the Dirac distribution and f_p=10Hz is the peak frequency. Fig. 13 shows a schematic diagram corresponding to this case. Homogeneous (zero) Dirichlet boundary conditions are applied on the four sides of the computational domain shown in Fig. 13, and no boundary condition is required at the layer interface. Here, we would like to mention that zero boundary conditions will produce reflections from the boundaries for longer simulations. In more realistic situations, the boundary reflections can be avoided by using absorbing perfectly matched layers [4,29]. To ensure the zero Dirichlet boundary condition, we have used $d_r=0.5/f_p$. Here, we have performed the numerical simulation of sound wave propagation in two-layered medium using EDP$_1$-C6 scheme with $\Delta x=\Delta y=12.5$m and $\Delta t=0.001$s.

Fig. 14 shows the computed sound fields at the indicated instants for a two-layered medium. Solutions at $t=0.3$s suggest that the computed wavefront forms a perfect circular shape before hitting the interface between two-layers. Moreover, by $t=0.65$s, the wavefront hits the interface, and part of the incident sound energy gets reflected while the other part gets transmitted in the bottom layer. As both layers are homogeneous, the reflected as well as refracted wavefronts are of the perfect circular form in the left half and the right half regions of the domain. Furthermore, both the reflected and refracted wavefronts propagate away as time advances, and the distance covered by the pressure pulse

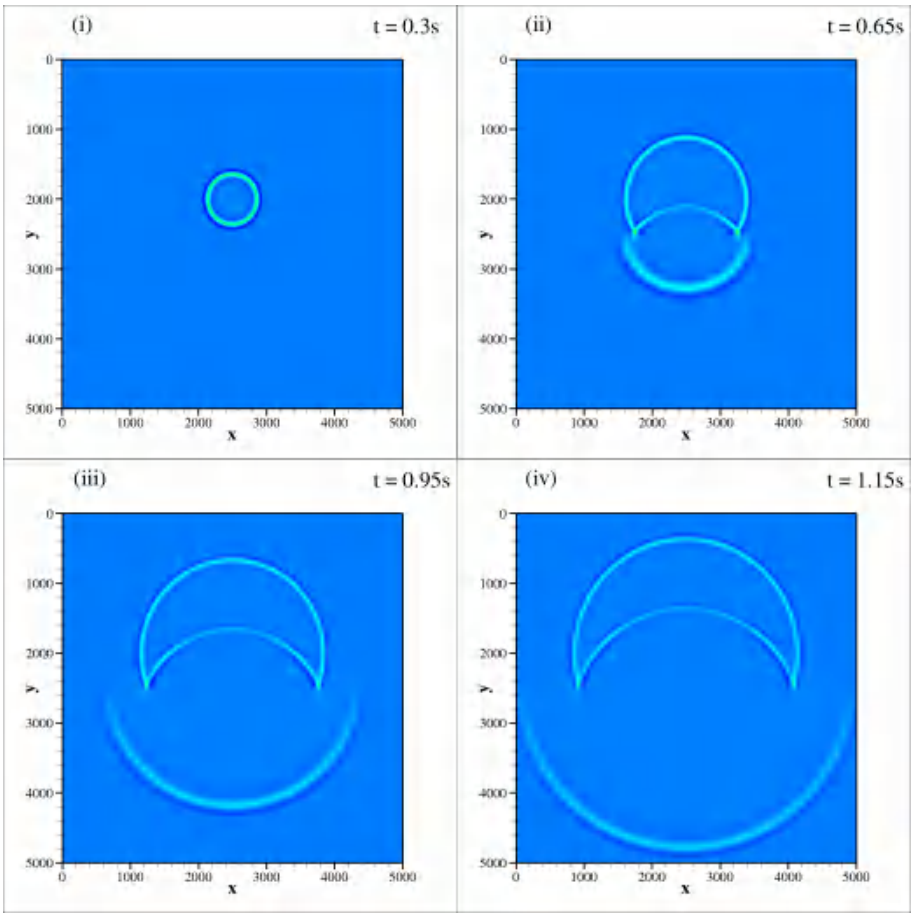

Figure 14: Development of sound fields in the two-layer medium at indicated instants using EDP_1-C6 scheme.

in the bottom layer is larger than the top layer. This is because the bottom layer's wave propagation speed is twice that of the top layer. It is also observed that the amplitude of the refracted wave in the bottom layer is relatively weaker than the reflected wave in the top layer. The wavelength associated with the sound wavefront in the bottom layer is twice that in the top layer, as the phase speed in the bottom layer is twice that in the top layer. Finally, we would like to emphasize that here the computed solutions are not able to reach the domain's boundary for the used time, thus we do not observe reflections from the boundaries in the present case.

5.2 Sound propagation in three-layered media

To further demonstrate the application of the EDP_1 time integration scheme in solving complex sound wave propagation problems in a heterogeneous medium, the corner-edge model [45] problem has been simulated. The 2D wave propagation in a heterogeneous

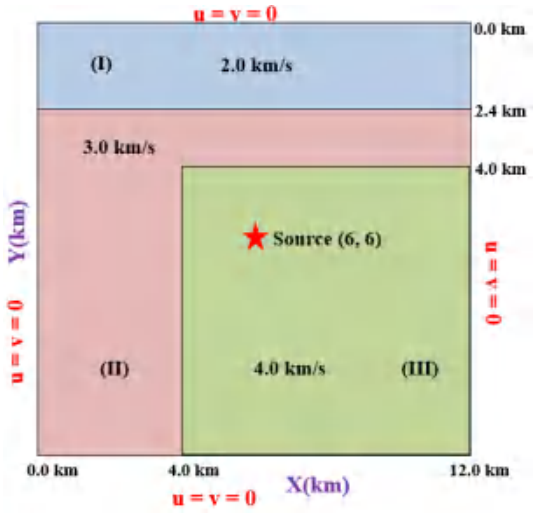

Figure 15: Schematic diagram for the corner edge model. The star indicates a sound source which has been located at the center of the domain.

medium as given by Eq. (2.5) has been solved in a domain that consists of three regions, I, II, and III. The phase speed of sound propagation in region I is 2.0km/s, 3.0km/s in region II, and 4.0km/s in region III. For performing simulation, we have considered a domain $(0,12000\text{m})\times(0,12000\text{m})$. The sound source has been prescribed as

$$f(t)=-5.76f_0^2\left[1-16(0.6(0.6f_0t-1)^2)\right]e^{(0.6f_0t-1)^2}.$$

The sound source has a peak frequency of $f_0=20Hz$ and is located at the center of the domain. Homogeneous (zero) Dirichlet boundary conditions are applied on the four sides of the computational domain shown in Fig. 15 and no boundary conditions are required at the layer interfaces. Here also we would like to mention that for large-time integration, zero boundary conditions will produce reflections from the boundaries, and in more realistic situations, the boundary reflections can be avoided using absorbing perfectly matched layers [4, 29].

For simulations, we have chosen a time-step of $\Delta t=0.006$s and the spatial steps of Δx=Δy=40m. Fig. 15 shows a schematic diagram corresponding to this case. Simulations have been performed using the EDP$_1$-C6 method, and the computed solutions at the indicated instants are shown in Fig. 16. The snapshot at $t=0.5$s shows the propagation of a sound wave with no reflections as the sound wave propagates inside an isotropic homogeneous region III. At $t=0.8$s, one observes the reflected and transmitted waves from the horizontal and vertical inner interfaces. The snapshots at t=1.2s and 1.5s display more complex wave fields than the previous snapshots. One observes the reflection and the transmission of sound waves from different inner interfaces. The four snapshots in Fig. 16 clearly show wave propagation phenomena, including reflection and transmission at horizontal and vertical interfaces in the corner-edge model without visible numerical

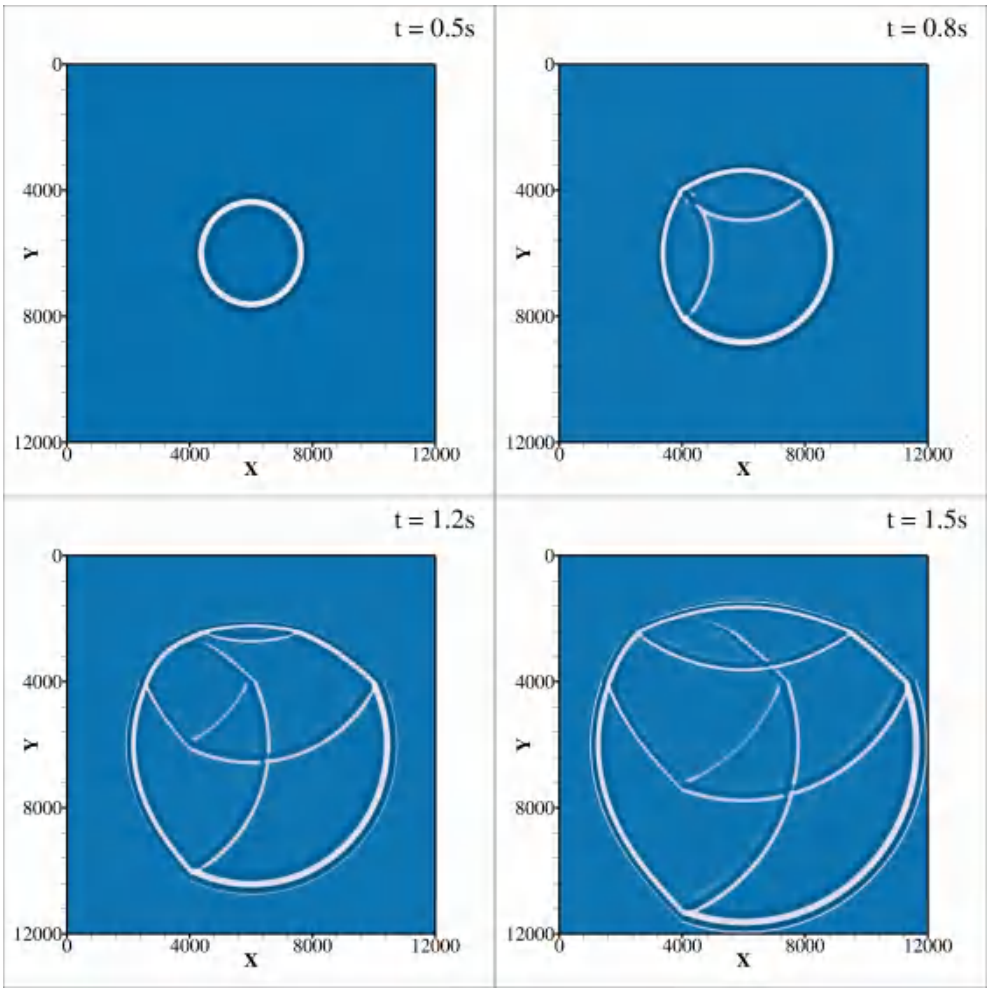

Figure 16: Development of sound fields in the three-layers medium with time has been shown using EDP_1-C6 scheme.

dispersion. As for the used time, computed solutions are not able to reach the domain's boundary, thus in the present case also, we do not see the reflections from the boundaries.

6 Simulations of 2D sine-Gordon equation

A soliton represents wave-like solutions to nonlinear dynamical systems that move across the medium without deforming due to dispersion. Moreover, a model representing the Josephson junction [20] can be described by the 2D sine-Gordon equation admitting soliton solution [10]. Solitons have been demonstrated to play a pivotal role in nonlinear PDEs, and they appear as a solution for a variety of equations such as the

Korteweg–de Vries equation, the sine-Gordon equation, and the nonlinear Schrödinger equation. Condensed-matter physics, optical fibers, shallow-water waves, and Josephson-junction oscillators are just a few of the physical applications where solitons have been discovered. Moreover, solitons are also thought to be fundamental excitations in a class of fully integrable Hamiltonian systems described by nonlinear dispersive PDEs. The review article [18] provides an in-depth look at the soliton solutions for several well-known PDEs.

This section deals with numerical simulations of the 2D undamped sine-Gordon equation. Numerical solutions are considered for a Josephson junction described by a 2D damped sine-Gordon equation [31], given as

$$\frac{\partial^2 u}{\partial t^2}+\beta\frac{\partial u}{\partial t}-\frac{\partial^2 u}{\partial x^2}-\frac{\partial^2 u}{\partial y^2}=F(x,y)\sin u, \quad \beta\geq 0, \tag{6.1}$$

where u represents the phase of the soliton. Here, we have chosen the computational domain, as, $\Omega=\{(x,y),-a<x<a,-b<y<b\}$ and $t>0$, were $\beta>0$ is the damping coefficient and $F(x,y)$ denotes Josephson current density. We have considered Eq. (6.1) having $\beta=0$ and $F(x,y)=-1$ with initial and Neumann boundary conditions, as given in [15],

$$u(x,y,0)=4\tan^{-1}(e^{(x+y)}), \qquad (x,y)\in(-7,7), \tag{6.2a}$$

$$\frac{\partial u}{\partial t}(x,y,0)=-\frac{4e^{(x+y)}}{1+e^{(2x+2y)}}, \qquad (x,y)\in(-7,7), \tag{6.2b}$$

and

$$\frac{\partial u}{\partial x}(y,t)\Big|_{x=-7,7}=\frac{4(e^{(x+y+t)})}{e^{(2t)}+e^{(2x+2y)}}, \qquad y\in(-7,7), \quad t>0, \tag{6.3a}$$

$$\frac{\partial u}{\partial y}(x,t)\Big|_{y=-7,7}=\frac{4(e^{(x+y+t)})}{e^{(2t)}+e^{(2x+2y)}}, \qquad x\in(-7,7), \quad t>0. \tag{6.3b}$$

The exact solution of the Eq. (6.1) with initial and boundary conditions given in Eqs. (6.2)-(6.3) for zero damping coefficient $(\beta=0)$ is given as [15]

$$u(x,y,t)=4\tan^{-1}(e^{(x+y-t)}).$$

For numerical simulations, we have chosen mesh-step size $\Delta x=\Delta y=0.25$ and time-step size $\Delta t=0.001$. Spatial discretization is performed using the $C6$ scheme. Fig. 17 shows the comparison of numerical and exact solutions of the Eq. (6.1) at indicated instants. From Fig. 17 it is observed that numerical results match very well with the exact solution.

6.1 Numerical simulations of the superposition of two orthogonal line solitons

As soliton solutions exist in various nonlinear PDEs, physical applications of solitons have been found in shallow water waves, optical fibers, and Josephson junction oscillators. Furthermore, analytical solutions are no longer attainable in more realistic systems

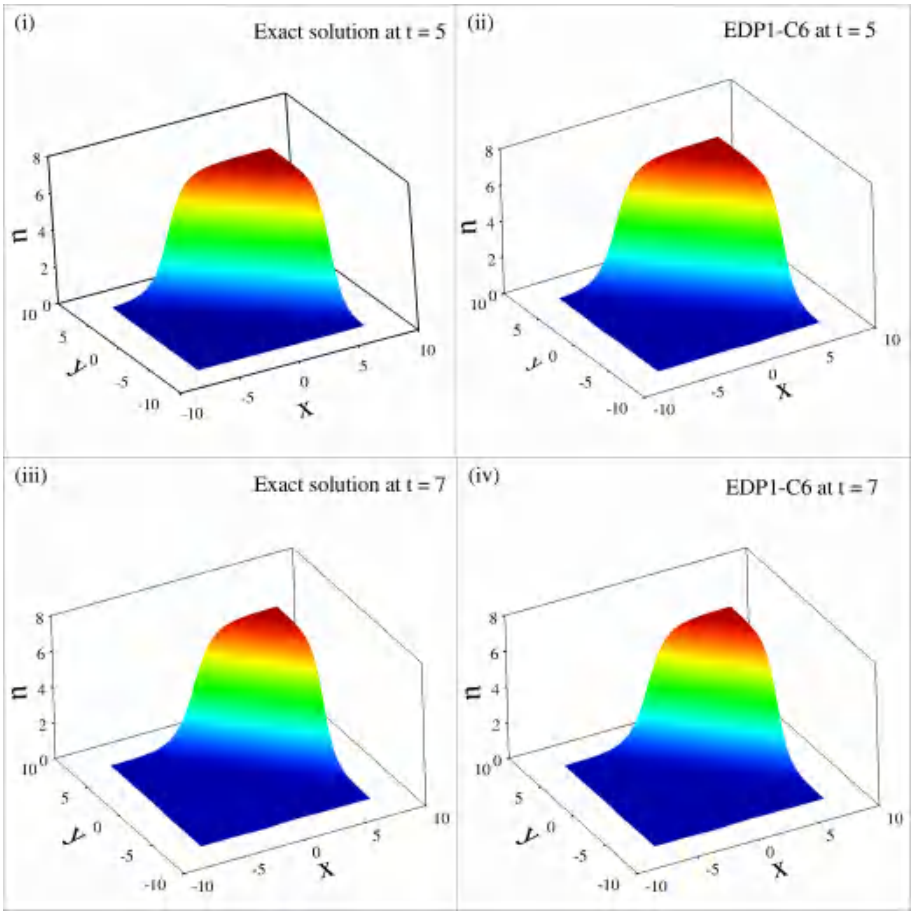

Figure 17: Comparison of numerical solutions obtained using EDP_1-C6 scheme with the exact solutions of undamped sine-Gordon equation given in Eq. (6.1) at indicated instants with initial and Neumann boundary conditions given by Eqs. (6.2)-(6.3), respectively. The value of damping coefficient $\beta=0$, Josephson current density $F(x,y)=-1$, $\Delta x=0.25$, $\Delta t=0.1$ and $c_1=1.48\times10^{-4}$.

with a damping effect from external forces, necessitating the use of numerical methods. The same holds for solitons or soliton-like formations in 2D or 3D, where the solitary waves' behaviors are mainly dependent on the number of space dimensions [3].

The superposition of two orthogonal line solitons is simulated using Eq. (6.1) with $\beta\neq0$ and $F(x,y)=-1$. The initial and boundary conditions [15] are chosen as,

$$u(x,y,0)=4\tan^{-1}(e^{(x)})+4\tan^{-1}(e^{(y)}), \qquad (x,y)\in(-6,6), \tag{6.4a}$$

$$\frac{\partial u}{\partial t}(x,y,0)=0, \qquad (x,y)\in(-6,6), \tag{6.4b}$$

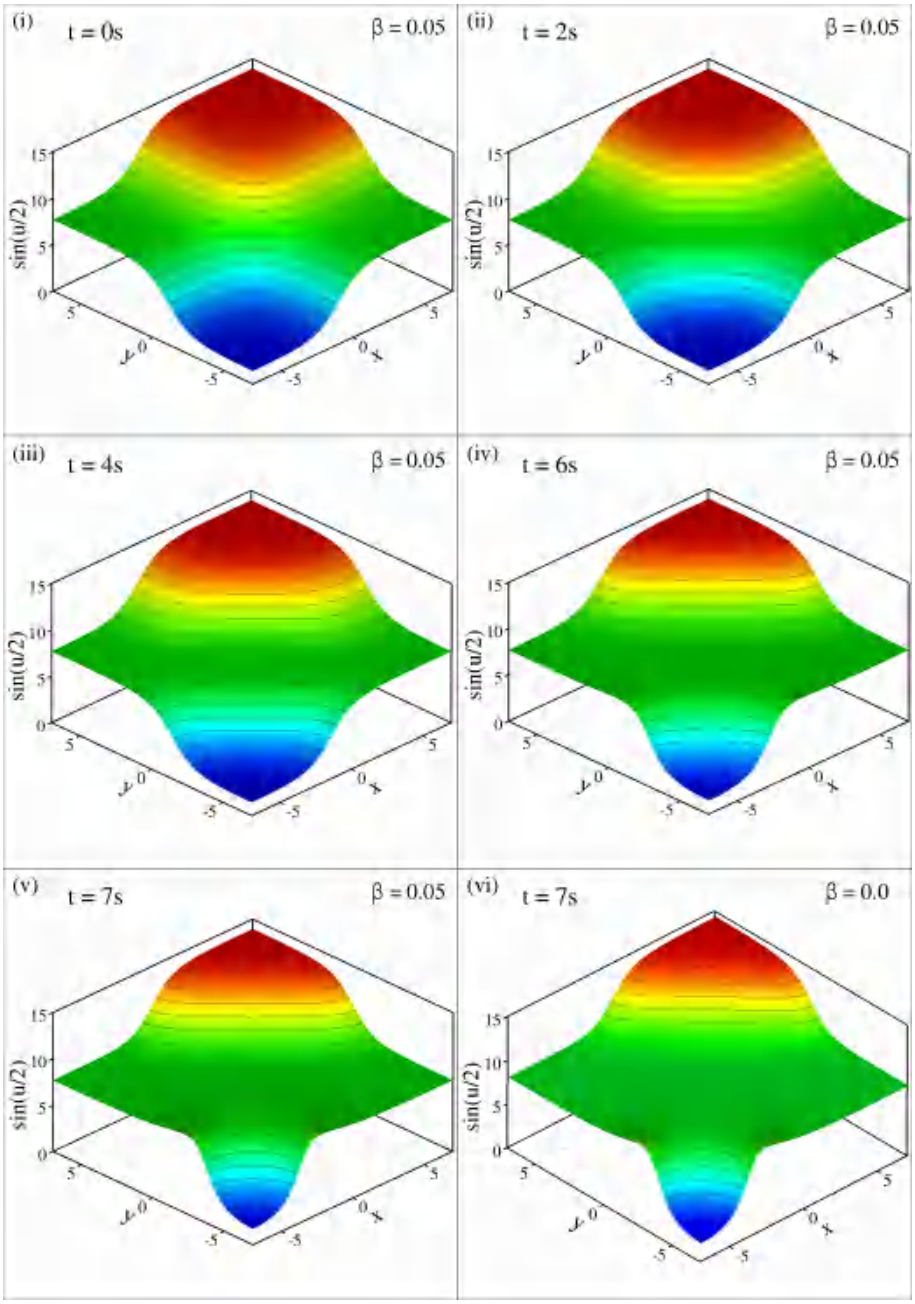

Figure 18: Breakdown of two orthogonal line solitons with initial and Neumann boundary condition given by Eqs. (6.4)-(6.5) at indicated instant using EDP$_1$-C6 scheme. Here, $\beta = 0.05$, Josephson current density $F(x,y) = -1$, $\Delta x = 0.25$, $\Delta t = 0.1$ and $c_1 = 1.48 \times 10^{-4}$.

and

$$\frac{\partial u}{\partial x}(y,t)\Big|_{x=-6,6}=0, \qquad y\in(-6,6), \quad t>0, \tag{6.5a}$$

$$\frac{\partial u}{\partial y}(x,t)\Big|_{y=-6,6}=0, \qquad x\in(-6,6), \quad t>0. \tag{6.5b}$$

Computations are performed with $\Delta x=\Delta y=0.25$, $\Delta t=0.001$ and $\beta=0.05$. Spatial discretization of the derivatives and homogeneous Neumann boundary conditions are accomplished using the $C6$ scheme. Numerical results shown in Fig. 18 indicate that the line solitons are moving away from each other along the $y=x$ line. The small value of damping coefficient (β) slows down the movement of orthogonal line solitons, which is also observed in the solutions shown in the bottom frames of Fig. 18 at $t=7$ with $\beta=0$ and $\beta=0.05$, respectively.

Moreover, taking the inner product of Eq. (6.1) with u_t and using the homogeneous Neumann boundary condition given by Eqs. (6.4)-(6.5), we have

$$\frac{\partial}{\partial t}\left[\frac{1}{2}\iint_{\Omega}\Big(u_t^2+|\nabla u|^2+2(1-\cos u)\Big)dxdy\right]=-\beta\iint_{\Omega}(u_t)^2dxdy, \tag{6.6}$$

where ∇u represent the gradient of u. From Eq. (6.6) it is evident that for the undamped $(\beta=0)$ sine-Gordon equation, the total (kinetic and potential) energy (E) given by

$$E=\frac{1}{2}\iint_{\Omega}\Big(u_t^2+|\nabla u|^2+2(1-\cos u)\Big)dxdy \tag{6.7}$$

remains conserved. However for damped case $(\beta>0)$, the total energy (E) is not conserved, and this term signifies the dissipation of energy from the system. The initial energy $(\text{at}\, t=0)$ is calculated over Ω by substituting initial conditions given in Eq. (6.4) into Eq. (6.7). The resulting expression for the initial energy (E_0) is given as

$$\begin{aligned}E_0=&8\left[\frac{b\left(e^a-e^{-a}\right)}{e^a+e^{-a}}+\frac{a\left(e^b-e^{-b}\right)}{e^b+e^{-b}}\right]+8\left[\frac{1}{1+e^{-2a}}-\frac{1}{1+e^{2a}}\right]\left[\frac{1}{1+e^{2b}}-\frac{1}{1+e^{-2b}}+b\right]\\&+8\left[\frac{1}{1+e^{-2b}}-\frac{1}{1+e^{2b}}\right]\left[\frac{1}{1+e^{2a}}-\frac{1}{1+e^{-2a}}+a\right]\\&+4\left[\sin 2\tan^{-1}(e^a)-\sin 2\tan^{-1}(e^{-a})\right]\left[\sin 2\tan^{-1}(e^b)-\sin 2\tan^{-1}(e^{-b})\right].\end{aligned}$$

Fig. 19 shows the energy conservation for damped and undamped sine-Gordon equation given in Eq. (6.1). In Fig. 19, frame (i) shows that the energy remains conserved for the undamped $(\beta=0)$ case and frame (ii) shows that energy decays for the positive value of the damping coefficient $(\beta=0.05)$.

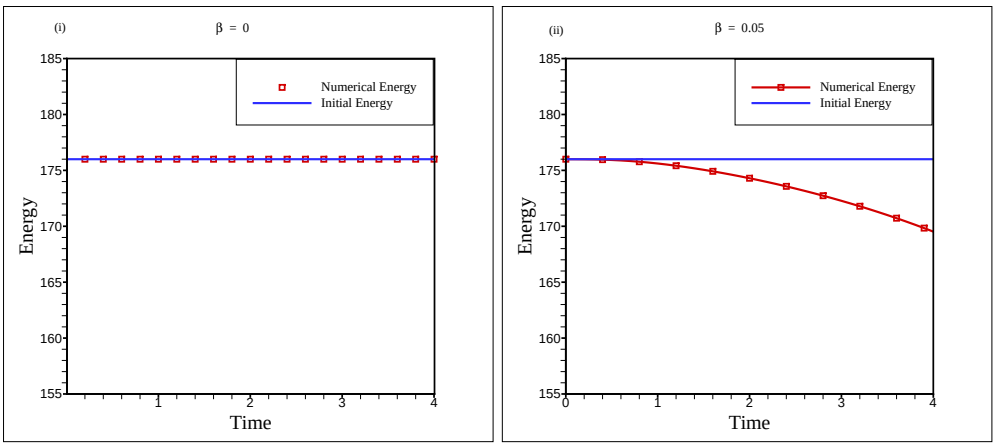

Figure 19: Energy conservation using EDP_1-C6 scheme for damped sine-Gordon equation with initial and Neumann boundary condition given by Eqs. (6.4)-(6.5). Here, $\beta=0.05$, Josephson current density $F(x,y)=-1$, $\Delta x=0.25$, $\Delta t=0.1$ and $c_1=1.48\times10^{-4}$.

7 Summary and conclusions

This paper has developed new dispersion relation preserving methods for sound and nonlinear wave equations having second-order derivatives in time. The Fourier stability analysis is used to assess the numerical properties of the present techniques. We have also compared the numerical properties of the developed method with the classical RK4 method, which confirms that the current methods outperform the RK4 method. Furthermore, we have also proved that the proposed method preserves energy, validated numerically by solving the damped and undamped sine-Gordon equation. Furthermore, to test the efficiency and robustness of the developed methods, we have also performed numerical simulations of sound wave propagation in homogeneous and two- and three-layered heterogeneous media. Numerical sound wave simulations show that the developed methods introduce less dispersion, phase-mismatch, and stability errors. Finally, numerical simulations of the damped sine-Gordon equation are performed for the case of line solitons, which validate that the proposed methods can depict the physical behavior of solitons in a very efficient manner.

Appendix: Consistency analysis

For the consistency analysis of the EDP_1 method, we have considered Eq. (2.3) in matrix form as

$$\frac{\partial}{\partial t}\begin{bmatrix} z \\ p \end{bmatrix} + A\begin{bmatrix} z \\ p \end{bmatrix} = O, \tag{A.1}$$

where, $A=\begin{bmatrix} 0 & -c^2\frac{\partial^2}{\partial x^2} \\ -1 & 0 \end{bmatrix}$ and O is a zero column matrix. By denoting $\phi=\begin{bmatrix} z \\ p \end{bmatrix}$, Eq. (A.1) can be written as

$$L\phi \equiv \frac{\partial \phi}{\partial t} + A\phi = O. \tag{A.2}$$

Next, using CD2 for spatial discretization in the semi-discretized system given in Eq. (2.4), we have

$$\frac{z_i^{n+1}-z_i^n}{\Delta t} - \frac{c^2}{\Delta x^2}\left(p_{i+1}^n - 2p_i^n + p_{i-1}^n\right) = 0, \tag{A.3a}$$

$$\frac{p_i^{n+1}-p_i^n}{\Delta t} - \left(c_1 z_i^n + (1-c_1) z_i^{n+1}\right) = 0, \tag{A.3b}$$

By using Taylor series expansion, Eq. (A.3) can be represented as

$$\begin{aligned} &\left[z_t - c^2 p_{xx}\right]_i^n + \mathcal{O}(\Delta t) + \mathcal{O}(\Delta x^2) = 0, \\ &\left[p_t - z\right]_i^n + \mathcal{O}(\Delta t) = 0, \end{aligned}$$

using vector notations, the above system can be represented as

$$\frac{\partial}{\partial t}\begin{bmatrix} z_i^n \\ p_i^n \end{bmatrix} + A\begin{bmatrix} z_i^n \\ p_i^n \end{bmatrix} + \mathcal{O}(\Delta t) + \mathcal{O}(\Delta x^2) = O. \tag{A.4}$$

Let $\phi_{\Delta t,\Delta x^2}=\begin{bmatrix} z_i^n \\ p_i^n \end{bmatrix}$, then Eq. (A.4) can be written as

$$L\phi_{\Delta t,\Delta x} \equiv \frac{\partial \phi_{\Delta t,\Delta x}}{\partial t} + A\phi_{\Delta t,\Delta x} + \mathcal{O}(\Delta t,\Delta x) = O.$$

Finally, from Eqs. (A.2) and (A.4) it is evident that $L\phi - L\phi_{\Delta t,\Delta x} \to 0$ as $(\Delta t,\Delta x) \to 0$. This proves that the EDP$_1$-CD2 method is consistent.

References

[1] Y. ADAMS, *Highly accurate compact implicit method and boundary conditions,* J. Comput. Phys., 24 (1977), pp. 10–20.

[2] A. R. APPADU, *Performance of UPFD scheme under some different regimes of advection, diffusion and reaction,* Int. J. Numer. Methods Heat Fluid Flow, 27(2017), pp. 1412–1429.

[3] J. ARGYRIS, M. HAASE, AND J. C. HEINRICH, *Finite element approximation to two-dimensional sine-Gordon solitons,* Methods Appl. Mech. Eng., 86 (1991), pp. 1–26.

[4] J.-P. BERENGER, *A perfectly matched layer for the absorption of electromagnetic waves,* J. Comput. Phys., 114 (1994), pp. 185–200.

[5] S. BRITT, E. TURKEL, AND S. TSYNKOV, *High order compact time/space finite difference scheme for the wave equation with variable speed of sound,* J. Sci. Comput., 76 (2018), pp. 777–811.
[6] D. CAROLAN, V. TUKOVIC, N. MURPHY, AND A. IVANKOVIC, *Arbitrary crack propagation in multi-phase materials using the finite volume method,* Comput. Mater. Sci., 69 (2013), pp. 153–159.
[7] W. CHEN, J. C. CHEN, AND E. Y. LO, *An interpolation based finite difference method on non-uniform grid for solving Navier-Stokes equations,* Comput. Fluids, 101 (2014), pp. 273–290.
[8] W. CHEN AND J. FISH, *A dispersive model for wave propagation in periodic heterogeneous media based on homogenization with multiple spatial and temporal scales,* J. Appl. Mech., 68 (2001), pp. 153–161.
[9] B. M. CHEN-CHARPENTIER, *An unconditionally positivity preserving scheme for advection-diffusion reaction equations,* Math. Comput. Model., 57 (2013), pp. 2177–2185.
[10] P. L. CHRISTIANSEN AND P. S. LOMDAHL, *Numerical study of 2+1 dimensional sine-Gordon solitons,* Physica D: Nonlinear Phenomena, 2 (1981), pp. 482–494.
[11] G. COHEN AND P. JOLY, *Construction and analysis of fourth-order finite difference schemes for the acoustic wave equation in nonhomogeneous media,* SIAM J. Numer. Anal., 33 (1996), pp. 1266–1302.
[12] M. CUI, *High order compact alternating direction implicit method for the generalized sine-Gordon equation,* J. Comput. Appl. Math., 235 (2010), pp. 837–849.
[13] M. DEHGHAN AND A. SHOKRI, *A numerical method for solution of the two-dimensional sine-Gordon equation using the radial basis functions,* Math. Comput. Simul., 79:700–715, 2008.
[14] D. DENG AND D. LIANG, *The time fourth-order compact ADI methods for solving two-dimensional nonlinear wave equations,* Appl. Math. Comput., 329 (2018), pp. 188–209.
[15] K. DJIDJELI, W. G. PRICE, AND E. H. TWIZELL, *Numerical solutions of a damped sine-Gordon equation in two space variables,* J. Eng. Math., 29 (1995), pp. 347–369.
[16] K. Y. FUNG, S. O. M RAYMOND, AND S. DAVIS, *A compact solution to computational acoustics, in: ICASE/LaRC workshop on benchmark problems in computational aeroacoustics,* NASA. Langley Research Center, ICASE (CAA), pages 59–72, 1995.
[17] E. HAIRER, S.P. NORSETT, AND G. WANNER, Solving Ordinary Differential Equations I: Nonstiff Problems, Springer-Verlag, Berlin, 1996.
[18] M. A. HELAL, *Soliton solution of some nonlinear partial differential equations and its application in fluid mechanics,* Chaos Solitons Fractals, 13 (2002), pp. 1917–1929.
[19] R. S. HIRSCH, *Higher order accurate difference scheme of fluid mechanics problems by compact differencing technique,* J. Comput. Phys., 19 (1975), pp. 90–109.
[20] J. D. JOSEPHSON, *Supercurrents through barriers,* Adv. Phys., 14 (1965), pp. 419–451.
[21] J. C. KALITA, *Effects of clustering on the simulation of incompressible viscous flows,* Eng. Appl. Comput. Fluid Mech., 1 (2007), pp. 36–48.
[22] J. C. KALITA, D. C. DALAL, AND A. K. DASS, *A class of higher order compact schemes for unsteady two-dimensional convection-diffusion equation with variable convection coefficients,* Int. Numer. Methods Fluid, 38 (2002), pp. 1111–1131.
[23] T. KAWAI, *Sound diffraction by a many-sided barrier or pillar,* J. Sound Vib., 79 (1981), pp. 229—242.
[24] L. E. KINSLER, A. R. FREY, A. B. COPPENS, AND J. V. SANDERS, Fundamentals of Acoustics, Wiley, 2000.
[25] G. KRISTENSSON, Second Order Differential Equations: Special Functions and Their Classification, Springer, New York, 2010.
[26] S. K. LELE, *Compact finite difference schemes with spectral-like resolution,* J. Comput. Phys., 103

(1992), pp. 16–42.
[27] K. Li, W. Liao, and Y. Lin, *A compact high order Alternating Direction Implicit method for three-dimensional acoustic wave equation with variable coefficient,* J. Comput. Appl. Math., 361 (2019), pp. 113–129.
[28] W. Liao, P. Yong, H. Dastour, and J. Huang, *Efficient and accurate numerical simulation of acoustic wave propagation in a 2D heterogeneous medium,* Appl. Math. Comput., 321 (2018), pp. 385–400.
[29] Q. H. Liu and J. Tao, *The perfectly matched layer for acoustic waves in absorptive media,* J. Acoust. Soc. Am., 102 (1997), pp. 2072–2082.
[30] B. Mahato, N. Ganta, and Y. G. Bhumkar, *Direct simulation of sound generation by a two-dimensional flow past a wedge,* Phys. Fluids, 30 (2018), 096101.
[31] B. A. Malomed, *Dynamics of quasi-one-dimensional kinks in the two dimensional sine-Gordon model,* Phys. D, 52 (1991), pp. 157–170.
[32] P. K. Maurya, M. K. Rajpoot, V. S. Yadav, and A. Singh, *New hybrid compact schemes for structured irregular meshes using Birkhoff polynomial basis,* J. Comput. Phys., 423 (2020), 109808.
[33] P. K. Maurya, V. S. Yadav, B. Mahato, N. Ganta, M. K. Rajpoot, and Y. G. Bhumkar, *New optimized implicit-explicit Runge-Kutta methods with applications to the hyperbolic conservation laws,* J. Comput. Phys., 446 (2021), 110650.
[34] Á. Nagy, I. Omle, H. Kareem, E. Kovács, I. F. Barna, and G. Bognar, *Stable, explicit, leapfrog-hopscotch algorithms for the diffusion equation,* Computation, 9 (2021).
[35] Á. Nagy, M. Saleh, I. Omle, H. Kareem, and E. Kovács, *New stable, explicit, shifted-hopscotch algorithms for the heat equation,* Math. Comput. Appl., 26 (2021), 61.
[36] J. Pradhan, Amit, B. Mahato, S. D. Dhandole, and Y. G. Bhumkar, *Construction, analysis and application of coupled compact difference scheme in computational acoustics and fluid flow problems,* Commun. Comput. Phys., 18 (2015), pp. 957–984.
[37] J. Pradhan and Y. G. Bhumkar, *Assessment of noise attenuation by thin reflecting barriers using dispersion relation preserving scheme,* Numer. Math. Theor. Meth. Appl., 12 (2019), pp. 942–968.
[38] M. K. Rajpoot, S. Bhaumik, and T. K. Sengupta, *Solution of linearized rotating shallow water equations by compact schemes with different grid-staggering strategies,* J. Comput. Phys., 231 (2012), pp. 2300–2327.
[39] M. K. Rajpoot, V. S. Yadav, J. Jaglan, and A. Singh, *Sound and soliton wave propagation in homogeneous and heterogeneous mediums with the new two-derivative implicit-explicit Runge-Kutta-Nyström method,* AIP Adv., 12 (2022), 075110.
[40] M. Saleh, E. Kovács, and Á. Nagy, *New stable, explicit, second order hopscotch method for diffusion-type problems,* Math. Comput. Simul., 208 (2023), pp. 301–325.
[41] T. K. Sengupta, Fundamentals of Computational Fluid Dynamics, Univ. Press (India) Pvt. Ltd., 2004.
[42] W. F. Spotz and G. F. Carey, *Formulation and experiments with high-order compact schemes for nonuniform grids,* Int. Numer. Methods Heat Fluid Flow, 8 (1998), pp. 288–303.
[43] C. K. W. Tam and J. C. Webb, *Dispersion-relation preserving finite difference schemes for computational acoustics,* J. Comput. Phys., 107 (1993), pp. 262–281.
[44] C. K. W. Tam, K. A. Kurbatskii, and J. Fang, *Numerical boundary conditions for computational aeroacoustics benchmark problem,* NASA Conference Publication 3352, (1997), pp. 191–220.
[45] P. Tong, D. Yang, and B. Hua, *High accuracy wave simulation–revised derivation, numerical analysis and testing of a nearly analytic integration discrete method for solving acoustic wave*

equation, Int. J. Solids. Struct., 48 (2011), pp. 56–70.
[46] R. VICHNEVETSKY AND J. B. BOWLES, Fourier Analysis of Numerical Approximations of Hyperbolic Equations, SIAM, 1987.
[47] J. VIRIEUX, *P-SV wave propagation in heterogeneous media: Velocity-stress finite-difference method,* Geophysics, 51 (1986), pp. 889–901.